Application of Fourier Transforms to time-resolved ambient pressure spectroscopy operando studies of CO oxidation over Pt(111)

GRIGORE-LEON RATIU

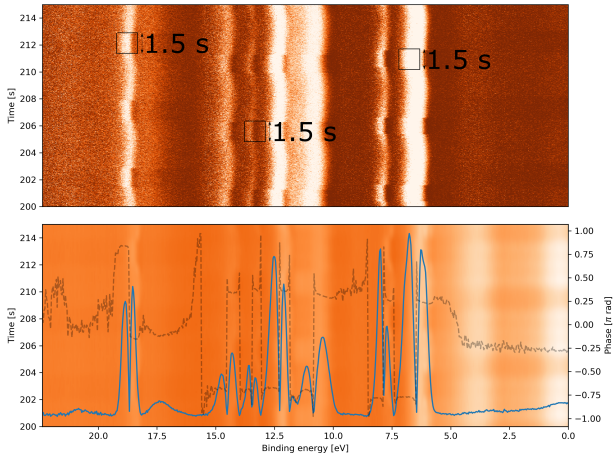

SUPERVISOR : JAN KNUDSEN

PROJECT CREDITS: 60 ECTS (HP); PROJECT DURATION: 12 MONTHS

THESIS SUBMITTED FOR THE DEGREE OF MASTER OF SCIENCE

DATE OF EXAMINATION: DECEMBER 2023

LUND UNIVERSITY

FACULTY OF SCIENCE

Lund University, Department of Physics - Division of Synchrotron Radiation Research

Abstract

The study of heterogeneous catalysis has important implications in increasing the efficiency of industrial processes and in reducing the emissions of greenhouse gases from sources such as automobiles. A reaction with high industrial relevance is the oxidation of CO on noble metal catalysts. In this work I apply Fourier Transformations to Ambient Pressure X-ray and Ultraviolet Photoelectron Spectroscopy and use this to study in situ CO oxidation over Pt(111) under pressure oscillation conditions generated by periodic dosing of CO pulses, with total pressure in the mbar regime, and at catalytic temperatures on the order of 580 ± 40 K. I demonstrate a high sensitivity of the method by showing evidence that 97% of the surface structure is static while 3% oscillates back and forth between different structural phases and show evidence that a fraction of the surface consistently becomes clean of adsorbates during the surface structure oscillations. Further, I demonstrate that Fourier Transformation-based methods provide excellent resolution in determining the work function shift impressed upon gas-phase species by structural oscillations on the catalyst surface. I confirm the ability of the new methods to discern the reaction mechanism of CO oxidation on Pt(111) for specific reaction conditions. Finally, I demonstrate the ability of Fourier Transform-based techniques to quantify the variation in catalyst electronic structure and discuss potential future developments for the methods employed. In the long run, this thesis helps with the validation and development of a potentially-valuable new analytic method for in situ heterogeneous catalysis studies.

Contents

Acronyms

AP - Ambient Pressure

DLD - Delay line detector

FT - Fourier Transform/ation

FFT - Fast Fourier Transform

MES - Modulation-excitation Spectroscopy

MFC - Mass Flow Controller

MFP - Mean Free Path

UHV - Ultra high vacuum

UPS - Ultraviolet Photoelectron Spectroscopy

XPS - X-ray photoelectron spectroscopy

1 Introduction

1.1 Motivation

Due to anthropogenic climate change, it is becoming increasingly important to lower world-wise CO_2 emissions from all sources, including emissions related to transportation and shipping. In reducing transportation-related emissions, transitioning to the use of electricity-powered vehicles is important; however, of notable importance is also the reduction of emissions from already-existing CO_2 sources.

Moreover, it has been shown [1] that air pollution is an important factor linked to a decrease in both quality of life and longevity, and with increasing urbanization, it is likely to remain an important factor. Since exhaust gases resulting from incomplete combustion are toxic, it is important both from a health and safety perspective to remove them as much as possible.

In light of this, the study of catalysis is important in order to achieve an understanding of the mechanisms underlying current emissions-reduction systems. With an improved understanding hereof, more efficient and ultimately cheaper systems can potentially be developed.

Catalytic systems present in motor vehicles are so-called heterogeneous catalysts, where the chemical species undergoing the reaction process are in a different phase - in this case, gaseous - than the catalyst - in this case, solid.

For instance, in car catalysts, some catalytic oxidation reactions of interest on noble metal catalysts are (not exclusively limited to) the oxidation of CO ($CO+\frac{1}{2}O_2 \rightarrow CO_2$), the oxidation of methane and other larger alkanes on catalyst surfaces ($CH_4+2O_2 \rightarrow CO_2+H_2O$, CHx oxidation), and the reduction of various nitrous oxides ($NOx \rightarrow \frac{1}{2}N_2 + \frac{1}{2}xO_2$), etc. An interesting discussion here, given conflicting reports in the literature, and to which I end up contributing in this work, is whether the surfaces are truly metallic or oxide-covered.

1.2 Surface science in the (static) study of catalysis

Since these catalytic reactions occur on surfaces, surface science methods are necessary to elucidate the mechanisms behind them. To develop our understanding, analysis of simple systems is undertaken. This is often referred to as *model catalysis*. The reason why we are interested in model catalysts is manifold, but the main considerations include: a) the fact that real catalysts are complex systems with several different elements and surface phases, thus complicating a systematic analysis; and b) real catalysts are not necessarily conductive, which is a requirement for many electron-based techniques including X-ray photoelectron spectroscopy (XPS), which is the main technique used in my work. Several other tools are also available - for example, Low-energy electron diffraction (LEED), scanning tunneling microscopy (STM)[2], etc. - to selectively probe catalytic surfaces. XPS is particularly useful as it is both elementally and chemically sensitive via examination of the so-called *chemical shift*, which is further explained below. Additionally, it is very surface-sensitive, which helps to reduce the background signal due to the (catalytically) non-interesting substrate material.

Traditionally, in the context of studying catalysis from the perspective of surface science, several categories of XPS studies must be distinguished. The first, and most basic, are static ultra-high vacuum (UHV) XPS studies.

I refer here to them as static because the parameters under which photoelectron spectra are recorded are unchanged. Each spectrum is recorded while the surface is already in an equilibrium condition.

Common parameters to vary are pressure (when doing in situ experiments, see below), temperature, gas flow, etc.

In classic XPS set-ups, pressure limitations are caused by the short mean free path (MFP) of photoelectrons in gases which is on the order of 1 mm (at a pressure of around 1 mbar). Therefore, catalytic surfaces have had to be studied under UHV conditions, hence at pressures below 10^{-8} mbar, where the MFP increases to the order of tens of cm. Moreover, the electron analyzers used to measure the kinetic energies of photoelectrons ejected from XPS samples traditionally contain multi-channel plates which are powered by high voltages, leading to sparking at pressures above 10^{-5} mbar. Nowadays, techniques have been developed (see the Experimental set-up section below) to allow for in situ studies, that is, studies of the catalytic reaction where the pressure conditions are closer to those found in real-world environments, approaching the mbar regime. Such in situ studies are extremely important, since the surface structures which form on catalytic surfaces under in situ conditions can in principle be different from those which occur under UHV conditions and the reaction mechanisms may change.[3].

As an example of prior work on Pt(111) under static in situ conditions, Calderón et al.[4] examine the near-ambient pressure CO oxidation on Pt(111) at various temperatures and with the application of a temperature ramp. While such experiments are dynamic in the sense that reaction conditions change and spectra are recorded under various experimental parameters, they are static in the sense that each spectrum is recorded, individually, with a time resolution much lower than the time scale at which surface reconstruction occurs (see further below). Indeed, Calderón et al. extract, for instance, information regarding the reaction ignition temperature (when CO_2 production picks up, based on XPS signal intensity), for which gas mixing ratios (CO:O) the reaction proceeds optimally, and how stable the reaction is in the long-term.

Sometimes, in situ studies are combined with ex-situ studies and involve more than one method of measurement. For instance, Miller et al.[5] examine the oxidation of CO on Pt(111) using both in situ XPS and ex-situ X-ray Absorption Spectroscopy (XAS). They report the formation of an extremely thin oxide on top of the Pt(111) surface before the onset of bulk oxidation. This highlights the fact that a so-called multi-modal approach proves to be the most robust in obtaining all available information from the study of a given system.

1.3 Time-resolved XPS studies and Fourier Transformation Ambient Pressure XPS

While static experiments as described above are useful in elucidating mechanisms behind catalytic reactions, it would be yet more useful to gain a deeper understanding of reaction dynamics and how the change in surface or electronic structure affects the change in catalytic activity of a surface. In this, time-resolved experiments are useful, as they enable the study of the time-evolution of each signal associated with a certain geometric or electronic structural state of the catalyst surface. As highlighted by Kalz et al. [6], this is likely to prove useful in the future for designing catalytic systems accounting for variations in reaction conditions.

The individual steps in the catalytic cycle occur in the μs to ps regime (see Figure 1), while the larger structural variation on the surface occurs in the ms regime. As mentioned above, one of the possible parameters to vary in order to induce a surface phase during in situ studies is the gas composition in the reaction cell. While it is in principle possible to probe the surface with ps time resolution and therefore resolve individual steps in the catalytic cycle, it is not possible to pulse gas into the reaction cell with such high time resolution. It is therefore to the ms regime

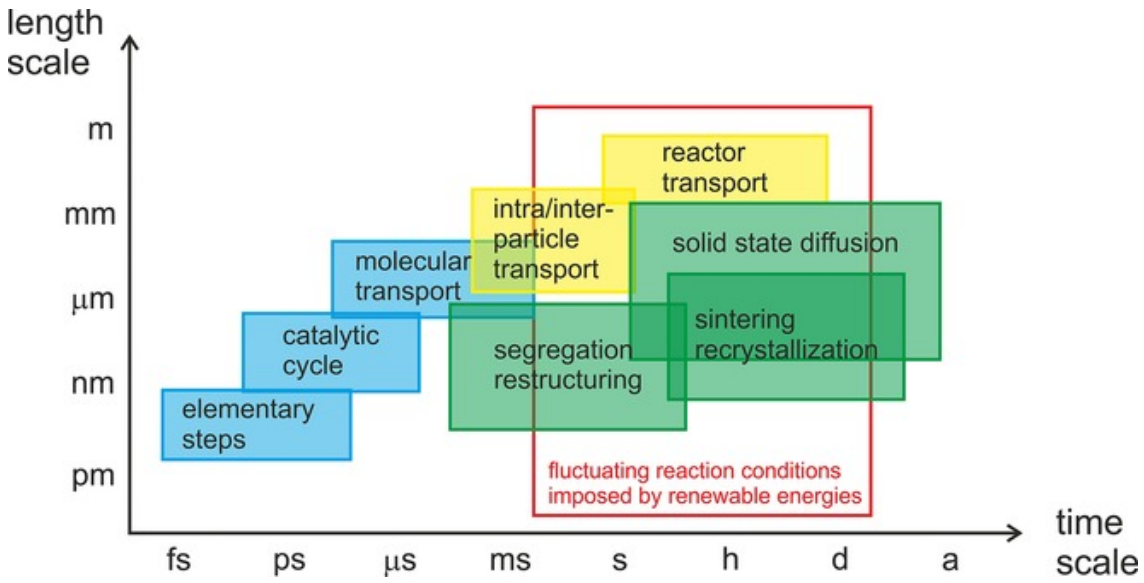

Figure 1: Dimensional scales for catalytic processes, in time and space. Taken from [6]

that we restrict our work. The gas pulsing will still cause a surface phase oscillation which can be resolved and analyzed. It is important to note, however, than unlike with other surface-sensitive techniques (LEED, STM, etc.), the flux (of photoelectrons) is quite low in XPS resolved with high time-resolution, and is made even lower by the experiment being performed under ambient-pressure conditions (again due to the photoelectrons having a low MFP in gas); the photon flux is important when performing quantitative analyses of the data, and therefore a challenge arises: *how does one improve the signal-to-noise ratio (S/N) in time-resolved APXPS?*. Ideally, we would like to have a technique which can distinguish majority spectator surface phases from minority catalytically-active phases. To understand why this is important, consider the following hypothetical situation: one surface species covers 90% of the surface but is catalytically-inert, while another species, which is catalytically-active, oscillates in coverage between 5% and 10%, with the remainder of the surface staying clean. In a non-time-resolved XPS experiment, the average spectrum will be dominated by the species with 90% coverage, and the oscillation of the catalytically-active species will be very hard to observe.

Knudsen et al. discuss event-averaging[7] as a possible solution to this issue of low S/N inherent to high-frequency time-resolved APXPS, which allows for the resolving of spectral features and chemical shifts in the binding energy due to changes in the surface phase of the catalyst. To understand this work, it is crucial to understand the notion of event-averaging. Knudsen et al. manage to quickly obtain snapshots of XPS spectra with sub-second time resolution. This signal, though distinguishable from noise, is quite weak. Using an internal trigger signal and an image-recognition algorithm, the recorded spectra can be separated in time, and the many-cycle signal can be reduced to an average one-cycle signal equivalent to one single surface phase cycle. The difference is evident even with a cursory examination by eye. Consider Figure 2, where in (a) one cycle is shown, and in (c) the event-averaged version of 58 pulses is presented as a comparison. The S/N ratio is much better, the spectral image is much clearer and conclusions are readily drawn. However, even though the relative times when the different components of the signal appear in the XPS signal are distinguishable, one needs to employ quantitative analysis to tools to ascertain how much the signal changes over any one cycle, and moreover one needs to have sufficient S/N to obtain a lock-in signal should internal

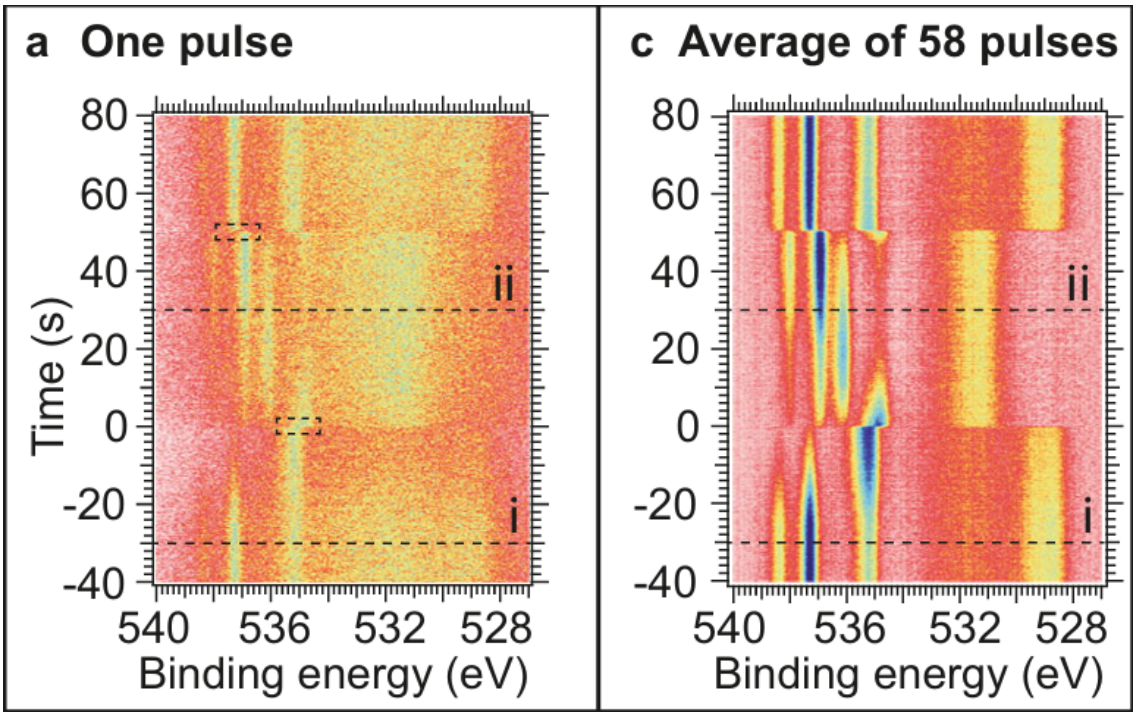

Figure 2: The effect of event-averaging on the signal-to-noise ratio in a time-resolved XPS experiment. Shown are the oxygen 1s core-orbital energy levels. Figure from [7].

triggering signals be employed.

The time resolution achieved by Knudsen et al. using the internal signal in the data was around 60 ms. More recently, Shavorskiy et al. achieved sub-ms time-resolution in a pulse-probe experiment using a different triggering scheme [8]. That is, they used a CCD camera with a fast shutter as a detector and wired the shutter to the piezo valve (see methods section) used to introduce gas pulses into the experimental cell. This allowed short-term exposures and enabled a time-resolution of 20 μs. The downside to this is low detector efficiency: of the total time used to run the experiment, below 1% was used to actually acquire spectra. This short exposure time, which is much lower than the pulsing period (100 ms) leads to long detection downtimes.

Building directly upon their earlier event-averaging work, Knudsen has recently developed a new analytic method based on Fourier transformation of the signal obtained during a pulse-probe experiment in a **t**ime-**r**esolved **A**mbient-**P**ressure **X**-ray **P**hotoelectron **S**pectroscopy (tr-APXPS) experiment. This method was demonstrated for CO oxidation over Pd(100). In so doing, one obtains both quantitative information regarding the change in intensity of the probed core-level peaks, as well as information regarding the relative positions in time of the signals corresponding to each surface state the surface progresses through. This information may then be directly employed to examine the relative times of formation and coverage evolution of adsorbates onto the metal surfaces, as well as their desorption back into the gas phase. The new method has tentatively been named Fourier Transform Ambient Pressure X-ray Photoelectron Spectroscopy (FT-APXPS). A major advantage of this method over the earlier event-averaging approach is that the magnitude of the Fourier Transform is directly related to the percentage of surface atoms which undergo a phase change. That is, the static and dynamic parts of the signal are readily separated. To exemplify this in practical terms, consider a sample whose surface is only partly subject to phase changes. In normal XPS, we

would probe the surface composition averaged over the beam focal spot and therefore get signal from all present surface species, regardless of what percentage of the surface actually undergoes a phase change. In addition, we also probe, as with regular XPS, the *gas phase* residing above the sample, that is, we ionize the gas molecules/atoms directly above the sample surface, and also obtain a signal from them. With FT-APXPS, we will then be able to see exactly how much of the surface changes in the form of the FT magnitude in relation to the XPS signal, and how much the gas composition changes. In addition, we mentioned above the problem of distinguishing minority surface species which oscillate from majority static species. This is elegantly resolved by considering the FT, as this will eliminate the static components in the XPS signal.

This, in principle is referred to in the literature to as *modulation-excitation spectroscopy* (MES) [9]. The modulation is represented by an induced change in external parameters, such as in our case the gas composition in the reaction cell, and the excitation is represented by a change in XPS signal. First proposed by Baurecht et al. in 2001 in the context of Infrared Spectroscopy, MES proposes treating a time-dependent, assumed-periodic signal at each point of interest E on a spectrum, $I(E,t)$, from a spectroscopy experiment as follows: introduce an arbitrary phase ϕ_k and define the component

$$A_k^{\phi_k}(E) = \frac{2}{T}\int_0^T I(E,t)\sin(k\omega t + \phi_k)dt \tag{1}$$

and then look at the different spectra varied as a function of the chosen ϕ_k, with $k \in \mathbb{Z}$ dictating which harmonic of a signal with oscillation frequency ω we try to match to the event-averaged signal[1] The signal $I(E,t)$ is an event-averaged signal. This is in practice a convolution between the event-averaged signal and a periodic harmonic function. In principle, this convolution could have been performed with any periodic or non-periodic function, but in this case, it determines how well the signal matches the period and phase of the function it is convoluted with. That is, the term $A_k^{\phi_k}$ as given in Eq. 1 is larger if $I(E,t)$ has more of its value in-phase with $\sin(k\omega t + \phi_k)$ and smaller if it is out of phase.

It is worth taking a moment and systematically re-examining why our Fourier Transform-based approach is distinct to the one first proposed by Baurecht and Fringeli. In their work, they propose first averaging the signal over multiple periodic repetitions of the system (in a conceptually similar but technically distinct fashion to the work of Knudsen et al. on event averaging), and then demodulating this signal by convoluting it with a sinusoidal signal with arbitrary phase delay. In this way, they obtain a dependence of the (event-)average intensity (or absorption, in the case of their work) on wavenumber and phase delay. Mathematically, it is a transformation for time space to phase space. In terms of Fourier Transforms directly, the closest analogy is as follows: extracting the FT magnitudes at a given frequency and binding energy, $|\mathcal{F}(E_B)|$, artificially projecting them through a full period and obtaining the phase-dependent magnitudes

$$|\mathcal{F}(E_B,\phi)| = |\mathcal{F}(E_B)|\sin(\phi), \phi \in [0; 2\pi] \tag{2}$$

and then using this information to determine the relative developments of various surface phases by considering at which phase ϕ the signal associated with any one surface state is maximum. In our approach, we instead look at the Fourier Transform's magnitude and phase directly in order to ascertain how much of the surface is changing by comparing the average signal over many periods to the FT magnitude, and we obtain the reaction dynamics (relative existence of surface changes) from the FT phase. The main difference, then, is that the FT magnitude shows how much the signal

[1] It is my opinion that ϕ_k should then be a function variable rather than an index, but I choose to conserve the notation used by Baurecht et al., which has become common in literature.

is oscillating with a given frequency, while the term $A_k^{\phi_k}$ shows how synchronized the signal is with $\sin(k\omega t + \phi_k)$.

In the field of XPS, I am aware of at least one study[10] in literature applying the principles described by Baurecht. The excitation in this case consists in switching the gas which is pumped on top of a powder catalyst sample (Pd/Al_2O_3) from CO to O_2. This induces a change in the surface structure, which then generates a measurable shift in the XPS signal. In order to average the signal, instead of using event averaging with an internal trigger as Knudsen et al., Roger et al. used the arrival of a gas pulse as an external trigger signal. This in principle also leads to a significant increase signal-to-noise ratio. Afterward, they apply the phase-sensitive detection principles described by Baurecht and Fringelli. Looking at the Pd $3d_{\frac{5}{2}}$ peak, a clear shift is identified at the transition from oxygen flow to CO flow, corresponding to a shift in surface phase. Plotting the obtained spectra as a function of the phase in the demodulation signal leads to a confirmation of the fact that the two gas flow regimes are distinct and the surface smoothly transitions from one phase to the other. This is a useful result, however it is only part of a subset of the results which can issue forth from an analysis of the full data using Fourier Transforms.

Inspired by the work of Baurecht et al. and Roger, and building directly upon the work of Knudsen in developing FT-APXPS, in this work I present a discussion of improvements possible in the operando study of heterogeneous catalysis by employing the new FT-APXPS method to examine the model catalytic reaction of CO oxidation over Pt(111) at near-ambient pressure. In particular, I focus on relating the reaction dynamics derived first from examination of the core-level spectra of Oxygen, Carbon and Platinum to the dynamics visible in the valence band region. Therefore, this work is a combination of FT-APXPS building upon the method established by Knudsen, and FT-Ambient Pressure Ultraviolet Photoelectron Spectroscopy (FT-APUPS). To my knowledge, this is the first time FT-APUPS has been explored as a method. The goals of the work are to *validate* ***FT-APXPS*** *on a new model catalyst system (CO oxidation over Pt(111) as opposed to Pd(100))*, to *add to the body of existing knowledge regarding this model catalyst* and *further explore the potential of FT-based XPS techniques.* Finally, another goal is to *extend the use of FT analysis of photoelectron spectroscopy data into the valence band, and thereby perform an in situ study of the time dynamics of catalyst electronic structure by use of FT-APUPS,* ***validating the usefulness of FT-APUPS in the process****.*

It has been shown in particular in the case of bi-metallic catalyst systems [11] that the electronic state of the surface has great influence on its catalytic activity, and so it is reasonable to assume that the change in its electronic state will induce a measurable change in catalytic activity. While the work of Knudsen has been focused on applying FT-APXPS on core-level spectra, there is no theoretical reason why the technique should not be applicable to valence-band spectra or to other surface science techniques, particularly those where phase-sensitive detection has already been demonstrated, such as XRD, XAS, PM-IRRAS, etc.[12]. Therefore, it is with this that I concern myself. By extending FT-APXPS techniques to the valence band, we perform FT-APUPS (ultraviolet photoelectron spectroscopy) with the goal of *gaining an understanding of the trilateral relationship between catalyst electronic structure, geometric surface structure, and catalytic activity.*

This shift in the energy band of interest presents significant challenges and unique opportunities. For instance, while in the case of XPS, separate spectra can be recorded for the core levels of carbon, oxygen, etc., in the case of valence band spectra, all information is contained in the same binding energy region. On the one hand, this is useful as it allows us to gain a complete picture in what is essentially a single spectrum, while on the other hand, it is likely to be challenging to distinguish spectral signatures of different chemical species if they overlap. Furthermore, in the case of XPS,

we primarily probe the geometric structure of the surface, while with UPS, we probe the electronic structure. This allows us to correlate the latter with catalytic activity, which, as mentioned above, is a useful avenue of inquest in the development of novel catalysts.

1.4 Relevant surface reaction mechanisms

To understand the background of the work and therefore be able to place it into context with respect to previously-performed research, it is necessary to understand what is already known about the CO oxidation process over noble metal catalysts. Understanding regarding CO and O adsorption onto noble metal surfaces in general and onto Pt(111) in particular, and knowledge of previously-effected in situ CO oxidation studies over such surfaces are relevant.

Therefore, I present a short introduction to endow the reader with the requisite knowledge. Two accepted mechanisms for reactions on surfaces with chemisorbed structures exist, namely the Langmuir-Hinshelwood mechanism and the Eley-Rideal mechanism. The most common of the two is the Langmuir-Hinshelwood mechanism, wherethrough two reactant compounds, A and B, both individually bind (*adsorb*) onto the surface, whereupon they interact to form the reaction product C, which eventually desorbs from the surface back into the gas phase above the surface.

An alternative proposed mechanism - the Eley-Rideal mechanism - posits that only one species, either A or B, adsorbs onto the surface and thereafter reacts with the other species, again forming the reaction product C adsorbed onto the catalyst surface, which desorbs back into the gas phase.

Graphical depictions of the Langmuir-Hinshelwood and Eley-Rideal mechanisms are shown in Figure 3, taken from [13].

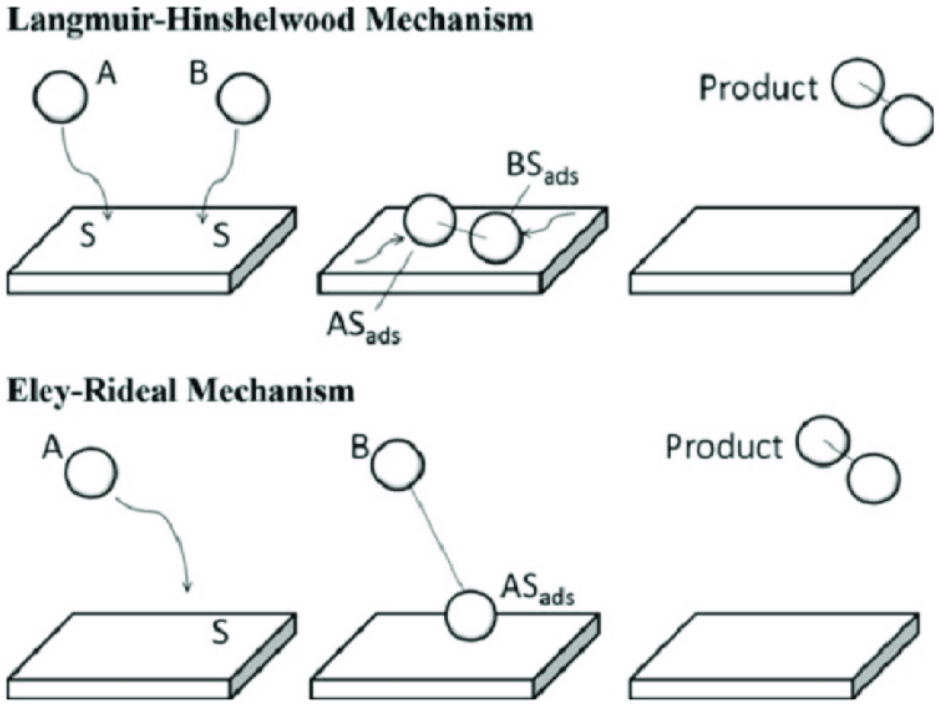

Figure 3: Graphical representation of the Langmuir-Hinshelwood and Eley-Rideal mechanisms. From [13]

1.5 CO Structures on noble metals

To specialize the discussion towards CO oxidation on Pt(111), it is first relevant to consider which adsorption structures *may* form on Pt. To this end, we consider the work of Björneholm et al. [14] and Johansson et al. [15].

On Pt(111), oxygen structure formation has been reported with the oxygen atoms adsorbing preferentially in three-fold hollow sites with a binding energy of the 1s core-orbital level of 529.4 eV, and forming a $c(2 \times 2)$ structure. By contrast, CO can adsorb in several configurations, in bridge or atop sites (O 1s energy levels of 531 eV and 532.7 eV, respectively; C 1s energy levels of 286 eV and 286.7 eV, respectively), starting with low-coverage (4×4) (low monolayer coverage (ML) of 0.19 ML) structures with preferential adsorption of CO in atop sites, and progressing, with an increase in pressure, to higher coverage structures such as $c(4 \times 2)$ and $c(5 \times \sqrt{3})$ [14], in which cases less favorable bridge adsorption sites are also occupied. In general, many different CO structures have been reported to form on Pt(111), in addition to the ones mentioned, with increasing ML coverages, such as $c(\sqrt{3} \times 2)$, $c(\sqrt{3} \times 5)$, and $(\sqrt{3} \times 7)$ (0.71 ML)[16]. At very high pressures, high density structures have been confirmed, such as a $(\sqrt{19} \times \sqrt{19})$ structure with 0.79 ML coverage [17]. These high-density structures are incommensurate Moire structures with adsorption *near* preferred sites.

In their work, Johansson et al. observed a rapid surface phase transition by pushing the system into a state such that all CO that is being pumped into the reaction chamber immediately adsorbs and interacts with the oxygen adsorbed on the surface, creating CO_2 which expands into a bubble above the reaction surface, in turn limiting the adsorption rate of CO and thereby limiting the reaction rate of its own production through reducing the amount of available surface-adsorbed CO. This reaction state where the production rate is limited by reactant availability is referred to as the Mass Transfer Limit (MTL) (in this case, CO-MTL). In more detail, the mechanism of the CO-MTL is as follows: at some point, the surface's catalytic activity increases to a limit such that all of the incoming CO which reaches the surface is instantly converted into CO_2. This leads to the formation of a CO_2 bubble above the catalytic surface. Therefore, the rate at which CO_2 is produced stagnates, and is thereafter limited by the diffusion rate of the CO gas through the CO_2 bubble.

The study by Knudsen et al.[7] that was discussed above, where the concept of event-averaging was introduced, is yet another example of an in situ study. There, information was recovered regarding the dynamics of the catalytic reaction and the authors were able to relate the change in surface structure to the catalytic activity of the surface. While in a single time-resolved spectrum the signal-to-noise ratio is too low to perform a quantitative analysis, by event-averaging, the signal-to-noise ratio is greatly improved, allowing the authors to determine that the catalytic activity is decreased by an oxygen-limited regime. In particular, they were able to demonstrate several key facts. The catalytic surface, in the high-pressure (3.2 mbar) regime, is initially oxide-covered. As CO is introduced to the sample cell, it is immediately converted to CO_2, as is also the case in the situation described above. However, now, with the increase in CO partial pressure, an oxygen depletion region forms above the surface, leading to an insufficient rate of oxide renewal. At some point, the surface very quickly (below detection resolution) switches from oxide-covered to CO-poisoned, and the catalytic activity drops. Therefore, the reaction is oxygen-limited, rather than CO-limited, as was the case with Johansson et al.'s study. This is due to the fact that this study was performed under different experimental conditions. This highlights both the power of the event-averaging technique and the fact that even a simple model catalyst reaction can have different limiting modes under different external conditions, evidencing the need for thorough investigations.

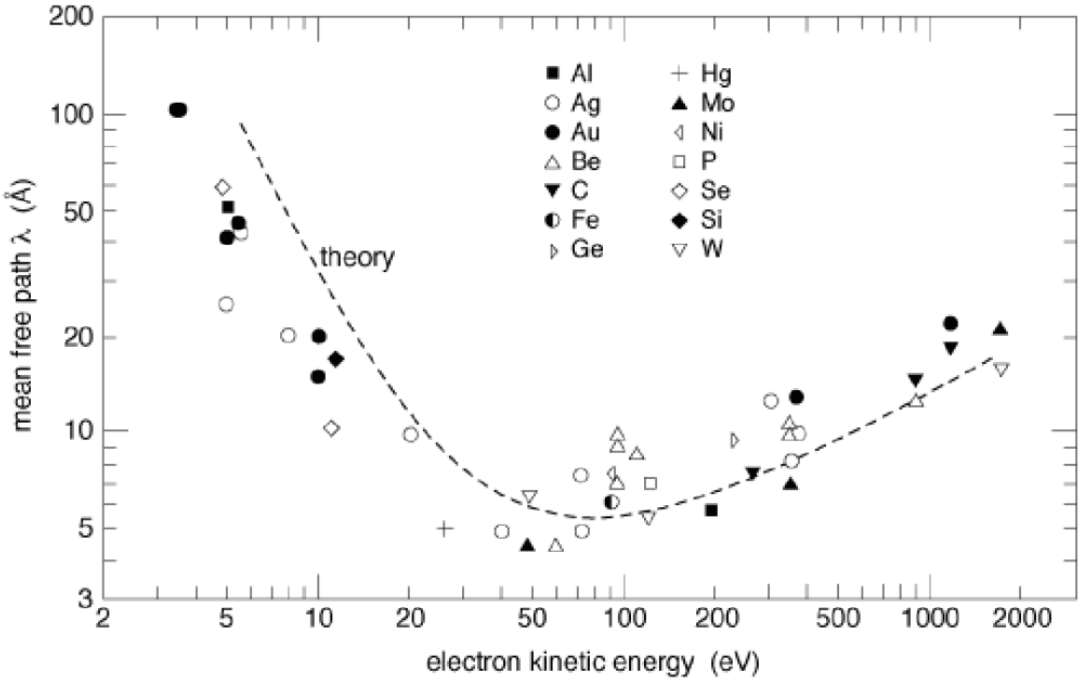

Figure 4: Example of an electron "universal curve", showing a material-agnostic dependence of the inelastic mean free path for electron-atom collisions depending solely on electron energy. From [19]

2 Theory and methods

2.1 X-ray photoelectron spectroscopy in UHV and at ambient-pressure

In order to perform studies of heterogeneous catalysis, good surface sensitivity is required of the technique employed. As the catalytic reaction is understood to depend mostly on the surface structure of the catalyst, a surface-sensitive technique is most appropriate in probing it. Indeed, AP-XPS is recognized as a premier technique for studying catalysis, as outlined in the introduction, and discussed in, for example, the review by Ogletree et al.[18]

When exposing a sample to a spectrally-pure beam of photons of sufficiently high energy (above the work function of the surface), electrons will be ejected from the sample surface, due to the photoelectric effect. For high enough photon energies, core-level electrons will also be ejected.

Crucially, electrons have a very short mean free path (MFP) in matter (on the order of 10 Å at the energies involved in XPS and 20 Å at the energies involved in UPS), which is most directly dependent on the energy of the electrons. This mean-free path is relatively independent of material, and so the general electron MFP dependence on energy is referred to as the *universal curve* (See Figure 4). This material agnosticism and short mean free path are what endow XPS with its desirable surface sensitivity and render it the ideal choice for heterogeneous catalysis experiments. Its downside, however, is that ultra-high vacuum (UHV) is required to perform XPS. Although the MFP of electrons in gases is much higher than in solids (on the order of 1 mm at 1 mbar), it is still very short and requires differential pumping inside the electron analyzer lens system in order to enable the electrons to reach the actual energy-dispersive detector.

The electrons ejected from a surface may then be used to obtain information about the structural

state of the surface. Indeed, while core-level electrons do not take part in chemical bonding, a small but finite and measurable so-called chemical shift is observed in their energy levels depending upon whether the atom to which the electron belongs is bonded to some other elements. For an example relevant to the present work on Pt(111), the bulk platinum atoms have electrons in the $4f_{\frac{7}{2}}$ orbital with binding energy $E_B = 70.9$ eV, while the surface atoms embedded on a clean surface have binding energy $E_B = 70.5$ eV, due to being surrounded by fewer neighbours (they have lower *coordination number*). If instead one considers surface Pt atoms with oxygen adsorbed in three-fold hollow sites, the binding energy of the Pt $4f_{\frac{7}{2}}$ electrons is instead $E_B = 71.12$ eV, as opposed to $E_B = 70.5$ eV, and this is what we call chemical shift.

In addition to examination of the core-level spectra of surfaces, photoelectron spectroscopy may further be employed to obtain the valence-band spectra thereof, whence information regarding the surface's electronic states may be obtained.

X-ray photoelectron spectroscopy is a highly-successful and expanding technique [2]. It was first pioneered by Karl Manne Siegbahn, for which he was awarded the Nobel Prize in physics in 1924[20]. His son, Kai Siegbahn, also worked on XPS and was also awarded the Nobel Prize in physics for his contributions, in 1981.[21]

Successful as it has been, however, the requirement for UHV also prevents XPS from fully documenting the catalysis reaction. As discussed previously, adstructures on the surface are different at higher pressures, and so a treatment at UHV conditions will not properly document a real system.

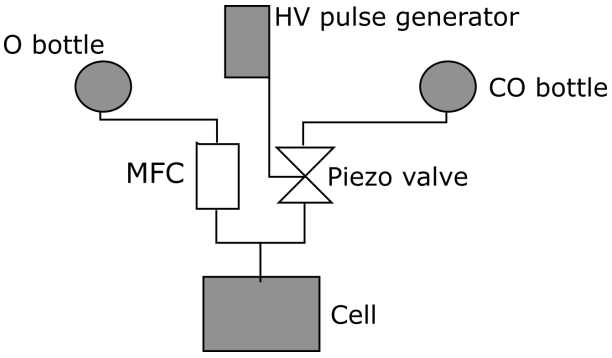

Figure 5: Figure showing the set-up of the gas lines to the experimental cell. The MFC is digitally-controlled while the Piezo valve is controlled via a high-voltage pulse generator which has to be manually-configured.

Later, technical developments have enabled the use of XPS techniques at (near-)ambient pressures. Chief amongst these advances have been the use of APXPS at synchrotron light sources whose high brilliance enable one to mitigate the loss in photoelectron flux due to collisions in the gas phase, and the use of differentially-pumped electrostatic lens focusing systems, which allow for a higher proportion of the emitted photoelectrons to be collected.[2][22]

2.2 Experimental set-up and conditions

All spectra for this work have been acquired at the SPECIES beamline of the MAX IV laboratory at Lund University in Sweden. The light source for the SPECIES beamline are elliptically polarized undulators mounted in the MAX IV 1.5 GeV storage ring. The light source provides a photon flux up to $\phi = 10^{15}$ s^{-1} in the energy region from $30 - 1500$ eV.[23]

The optics of the beamline are shown in Figure 6. I do not discuss the uses of the various components in detail as this is not within the scope of the present work.

For all spectra which will be shown in this work, the pulsing conditions are similar and outlined below. The sample is held at near-ambient pressures of $p \approx= 1.4$ mbar, in a constant flow of O_2 at a rate $Q_{O_2} = 3.5$ sccm and gas train pulses of CO are introduced with a frequency $f_{CO} = 0.2$ Hz,

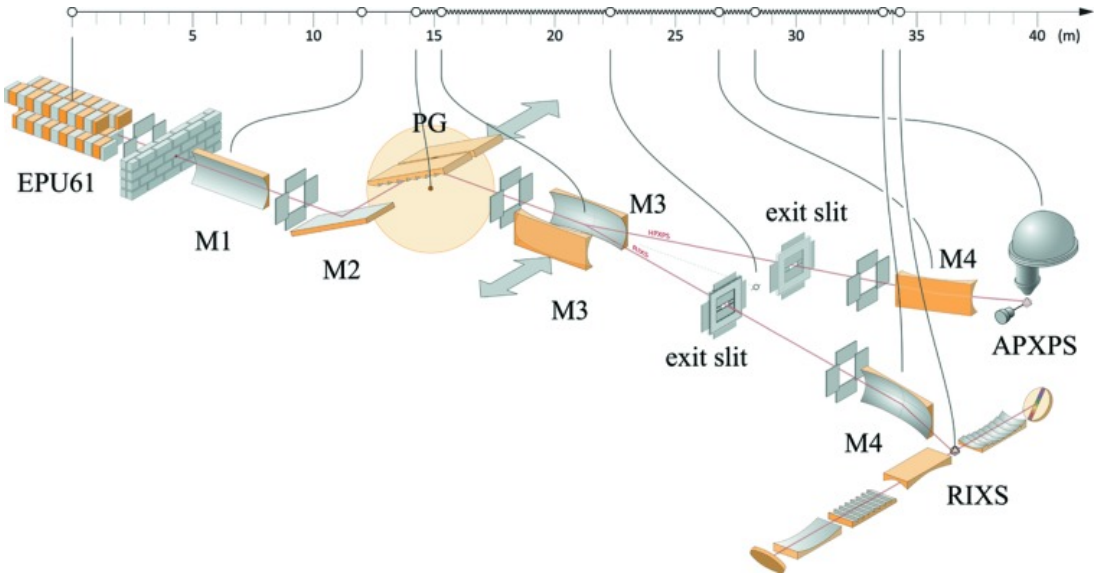

Figure 6: Figure showing the beamline optics set-up at the SPECIES beamline. Reproduced from [23].

therefore with a period $T_{\mathrm{CO}} = 5$ s. The duration (width) of the pulses is 100 ms in all cases. The temperature will be specified individually for each spectrum, but they are always around 580 ± 50 K.

The gas-pulsing set-up is composed of a mass flow controller (MFC) for the background O_2 flow and a piezo valve to enable rapid pulsing of CO gas. A rudimentary sketch of the set-up is shown in Figure 5.

Ìt is also useful to discuss the practical set-up of the measurement apparatus, as ambient-pressure XPS is relatively difficult to perform and requires specialized equipment. Therefore, I describe the end-station of the SPECIES beamline at which the present experiment has been performed.

The experimental cell design philosophy is known as the "Lund cell-in-cell" and is described by Knudsen et al. and Schnadt et al. [24][25]. The summary of this approach is as follows: the actual experimental environment is composed of a near-ambient-pressure cell which is placed inside of an UHV chamber. This enables ambient-condition study of chemical reactions through XPS and UPS. Since the ambient-pressure cell is removable, the instrument is then usable for both ambient-pressure and UHV measurements.

The electron analyzer used is a SPECS Phoibos 150 NAP, a schematic of which is shown in Figure 8. A schematic of the whole SPECIES APXPS end-station is shown in Figure 7 (a), with a close-up view of the ambient-pressure cell in (b), taken from [26]. Note the nozzle system designed to capture electrons and direct them into the differential pumping stage and electromagnetic lens system. The differential pumping stage has four different turbo molecular pump stages. The first stage reduces pressure by a factor of $10^3 - 10^4$. The lens system is meant to apply a retarding voltage to the photoelectrons so as to achieve optimal signal detection(see Electron analyzer transmission correct section). The hemispherical analyzer itself consists of two concentric hemispheres endowed with a potential difference, resulting in an energy-dispersive effect along one of the detector axes. The detector itself is a Surface Concept GmbH 3D-DLD4040-150 delay-line detector, consisting of multiple multi-channel plates (MCPs) in a stack with two layers of delay lines. The resolution of

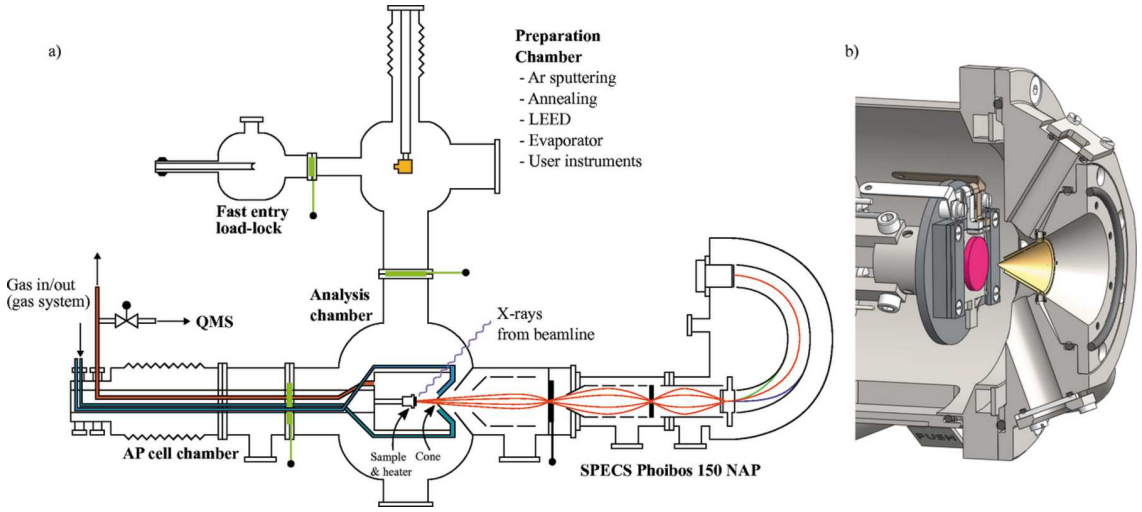

Figure 7: (a) General schematic of the APXPS end-station at the SPECIES beamline. (b) A close-up of the ambient-pressure cell together with the electron analyzer nozzle. From [26].

the detector is 800x1000 pixels.[26]

2.3 Data calibration and processing

In this section, I discuss the steps that I have taken in processing the raw data into experimental spectral data.

In the context of tr-APXPS, the electron analyzer is run in snapshot mode, which consists of the rapid ($\approx$ 75 Hz maximum sampling frequency) acquisition of spectra which can be used to construct an image over many gas-pulse cycles. An example of the resulting spectrum, for the core-level of C 1s scanned near a sample surface is shown in Figure 9.

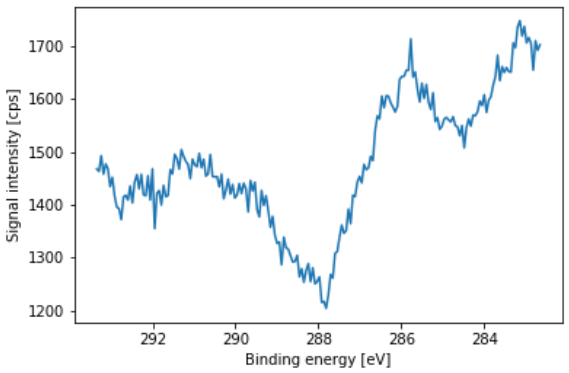

Figure 9: Average signal value of the C 1s (s) spectrum at each binding energy before applying the transmission correction.

This data needs to be calibrated in three main ways: firstly, transmission sensitivity differences in the electron analyzer need to be accounted for, and secondly, the gas-pulse-train-induced effects need to be removed from the data. Finally, the binding energy axis has to be calibrated to the Fermi edge. I go into detail regarding each correction below.

2.3.1 Fermi edge calibration and apparent binding energy of gas phase photoelectrons

I have mentioned before the binding energy of the atoms. It is time to be specific about the equations applicable to our case. The discussion in this section is based on work by V. Boix and U. Küst[19][28].

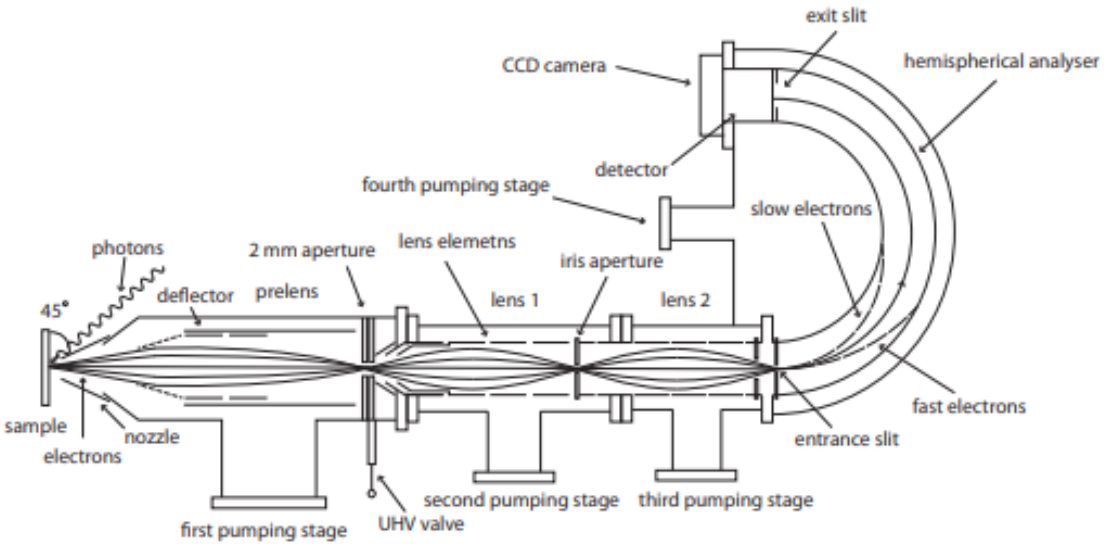

Figure 8: Schematic of the Phoibos NAP 150 analyzer, taken from [27]. The CCD camera has been replaced by a Delay Line Detector.

In XPS, the kinetic energy of the photoelectrons detected by the electron analyzer is related to the photon energy $h\nu$ used to eject the photoelectron, the binding energy of the electronic energy level whence the electron is ejected (for short, I will also use the term "photoelectron binding energy" to refer to this, even though this is not strictly correct, as the binding energy of the various electronic levels is a property of the atom and not of the electrons themselves.) E_B, and the sample and analyzer's potentials. If we let the work function of the experimental surface be denoted by Φ_S, then the kinetic energy at the sample surface of an electron ejected from an energy level with binding energy E_B is given in the simplest expression by [19]

$$E_K^{\text{surface}} = h\nu - E_B - \Phi_S \tag{3}$$

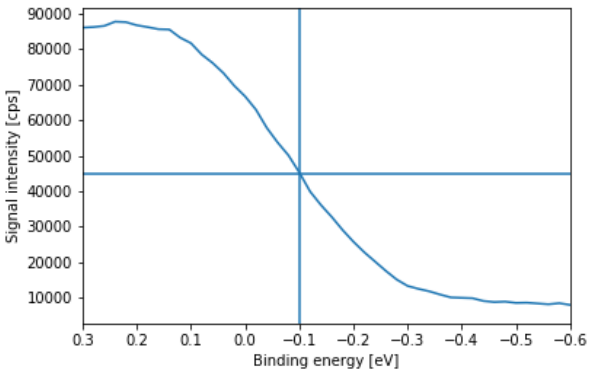

Figure 10: Finding the Fermi Edge for the C 1s (s) spectrum.

which must be augmented by consideration of the surface's Fermi level (with corresponding Fermi energy E_F) and the relative work functions of the sample surface and analyzer used to collect and focus the electrons onto a detector. Let us consider this more in-depth. Let the potential of the analyzer be Φ_A and the potential of the sample be Φ_S. Assume for convenience that $\Phi_A > \Phi_S$ in absolute terms. Once the photoelectrons have left the sample, they still need to overcome the potential difference $\Delta\Phi = \Phi_A - \Phi_S$ and their kinetic energy will therefore be reduced. Moreover, since we are only *guaranteed* to find electrons below the Fermi level at $T = 0$ K, and otherwise may find it for ambient temperature T at some energy E according to the

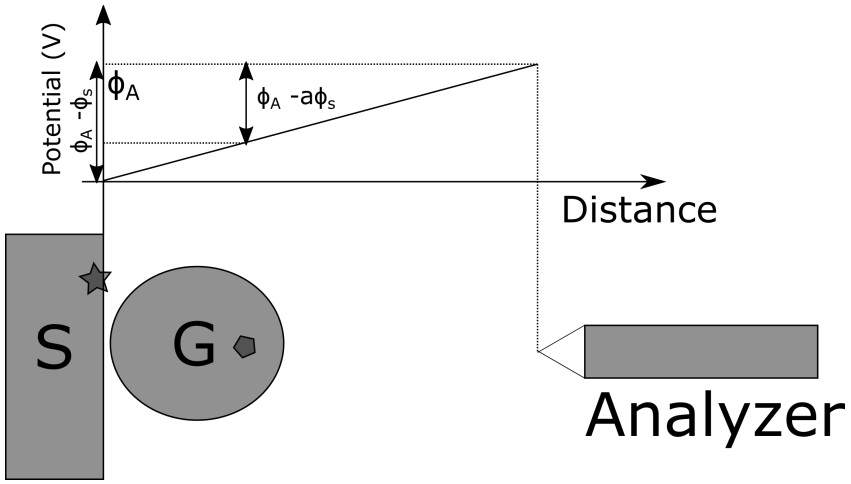

Figure 11: The potential differences ejected photoelectron have to overcome. When ejected from the surface (S) position, a photoelectron has to overcome the whole potential difference $\Phi_A - \Phi_S$, while if ejected from the gas phase (G) it would have to overcome a smaller potential difference $\Phi_A - a\Phi_S$.

Fermi-Dirac distribution

$$f(E) = \frac{1}{e^{\frac{E-E_F}{kT}} + 1}$$

we also need to calibrate for the Fermi edge. That is, around $E_B = 0$ ($E_B = 0$ is considered by definition to be the Fermi level), signal might commence slightly below or above the zero-point, and we must shift the spectrum accordingly. The signal has a sloped onset, and we select the binding energy with highest slope as the reference energy. An example of finding the Fermi Energy is shown in Figure 10. Therefore, when detected in the electron analyzer's detector, the kinetic energy of the electrons will be

$$E_K^{\text{analyzer}} = h\nu - BE - \Phi_S - \Delta\Phi = h\nu - BE - \phi_A \tag{4}$$

When an electron is ejected from the gas phase, it does not have to overcome a sample's work-function, *however* it still does have to overcome a potential difference. This potential difference will not be $\Delta\Phi$ and will instead be smaller. Figure 11 is instructive in this sense.

An electron ejected from S will have to overcome the entire potential difference $\Delta\Phi$, while an electron ejected from the region G will only have to overcome some smaller $\Delta\Phi_G < \Delta\Phi$. We assume that the potential increases linearly from Φ_S to Φ_A, and therefore it must be that $\Delta\Phi_G = \Phi_S - \alpha\Phi_A$, $\alpha \in (0, 1)$. Hence, for a photoelectron ejected from the gas, we have

$$BE = h\nu - E_K - (\Phi_A - \alpha\Phi_S) = h\nu - E_k - \Phi_A + \alpha\Phi_S \tag{5}$$

and so a finite shift $\delta\Phi_S$ inducing the change $\Phi_S \to \Phi_S + \delta\Phi_S$ will induce in this binding energy a shift

$$\delta\text{BE} = \alpha\delta\Phi_S \tag{6}$$

When it comes to the gas phase photoelectrons, there is no work function to account for, however, it follows from Eq. 5 that the binding energy detected by the analyzer is influenced by sample work function. When the surface structure of the sample changes, this changes the sample work function and, consequently, the binding energy of peaks observed in the gas phase will change.

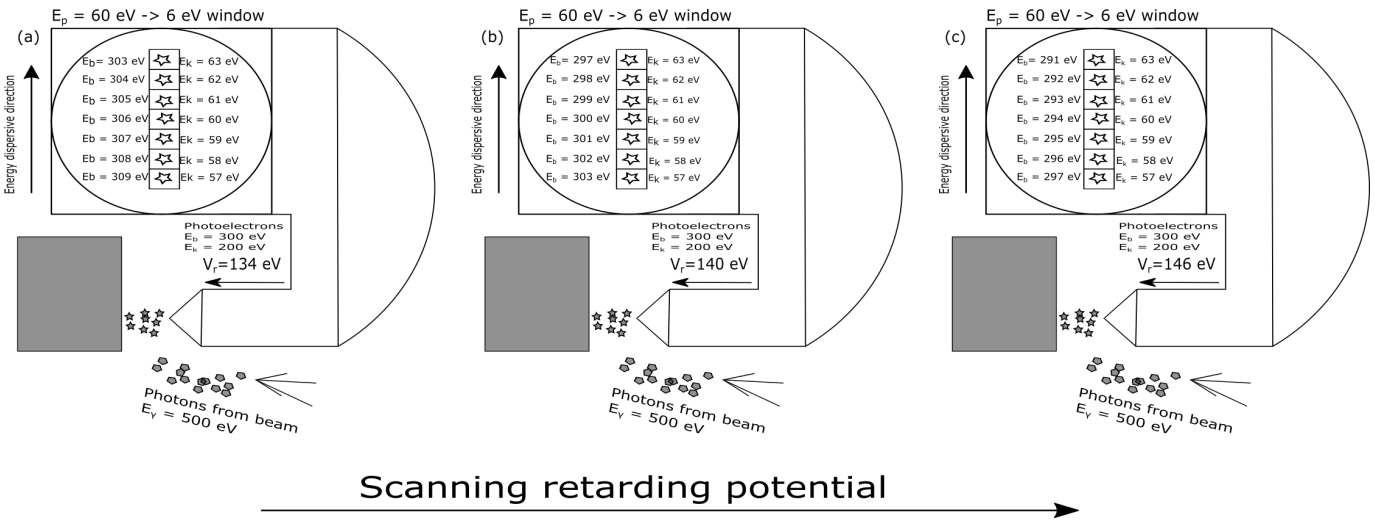

Figure 12: Figure showing the effect of scanning the retarding voltage on the electron analyzer. The ejected photoelectrons are supposed to have an energy distribution centred around $E_k = 200$ eV in this case.

2.3.2 Electron analyzer transmission correction

The electron analyzer delay line is a 2D detector with both an energy-dispersive axis, and another axis which can be set to preserve some other experimental parameter (for example, the emission angle of the photoelectrons, or the position on the sample whence a particular photoelectron originated). The detector is divided into bins along these two axes, with each bin corresponding to a given kinetic energy and a given secondary parameter. Every detector bin has a different sensitivity, and it is important to account for the error this introduces. Furthermore, the transmission of electrons to each bin is different.

In principle, so long as the secondary electron parameter is unimportant (for instance, doing pure energy-dispersive XPS and not angle-resolved XPS, etc.), it is fine to integrate over the non-energy-dispersive axis, so we will ignore it in what follows and use a single binning axis in the detector, to simplify the explanation.

The electron analyzer will allow electrons with a set kinetic energy $E^{e^-}_{\text{kin}}$ - known as the pass energy (E_p) - to hit the middle bin of the electron analyzer in the energy-dispersive direction. The window of the electron analyzer - that is, the total photoelectron kinetic energy range which passes through the hemisphere of the analyzer, is usually around 10% of E_p. Those electrons with a kinetic energy above E_p end up "above" the middle bin, and those with a kinetic energy below E_p end up "below" the middle bin (see, for instance, panel (b) of Figure 12).

As mentioned above, the kinetic energy of an electron with binding energy E_B extracted from the sample or the gas phase by a photon with energy $h\nu$ will in principle be related to its binding energy (ignoring, for the sake of convenience, the influence of the work functions of the analyzer and sample) via $E^{e^-}_{\text{kin}} = h\nu - E_B$. This might still be above the pass energy E_p. Therefore, the optics system of the electron analyzer is responsible, via its retarding voltage, to reduce the kinetic energy of the electrons until they E_p or within 10% of it for the photoelectrons with the binding energies of interest.

When operating in fixed mode, the electron analyzer will scan the retarding voltage such that all

photoelectrons with binding energies of interest will have all kinetic energies within the detection window. In other words, all binding energies will be detected in all bins of the electron analyzer in the energy-dispersive direction, and summed together, such that the effect of the MCP's varying bin sensitivity is cancelled out.

I exemplify this in Figure 12. Imagine, for the sake of convenience, that we aim to detect electrons with a binding energy of $E_B = 300$ eV, using photons with an energy $h\nu = 500$ eV. The kinetic energy is therefore $E_{\text{kin}} = 200$ eV upon exit from the sample. Suppose that we wish to use a pass energy $E_p = 60$ eV, and therefore necessarily a window of 6 eV. The bins then detect electrons with kinetic energies up to 63 eV and down to 57 eV. The retarding voltage of the optics system is initially set to $V_r = 140$ eV (panel (b)) and slows electrons down such that the kinetic energy of electrons with exactly $E_B = 300$ eV is exactly equal to the pass energy, and these electrons end up in the central bin, while those with a binding energy of 297 eV end up in the uppermost bin, and those with a binding energy 303 eV end up in the lowermost bin.

Now the retarding voltage is scanned from 134 eV (panel (a)) up to 146 eV (panel (c)). In the former case, the electrons with $E_B = 303$ eV are slowed from $E_k = 297$ eV to $E_k = 63$ eV and end up in the uppermost bin, while in the latter case, electrons with $E_B = 297$ eV end up with $E_k = 57$ eV and are therefore detected in the lowermost bin.

In this way, electrons with binding energies between 197 and 203 eV are detected in all bins of the analyzer.

In snapshot mode, however, the retarding voltage is *not* scanned, in order to facilitate the quick acquisition of spectral data, and this can (and from experience does) lead to issues wherein the varying sensitivity of the MCP bins significantly affects the resulting spectrum.

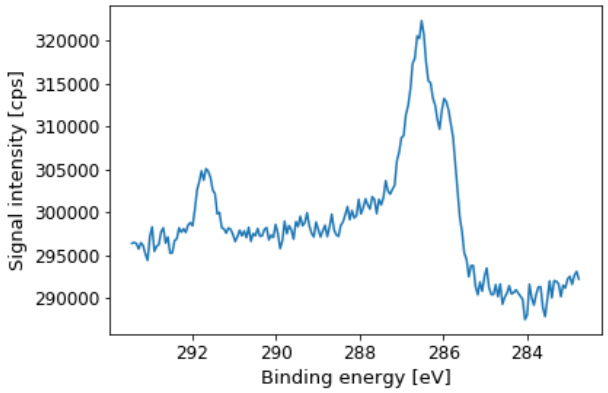

Figure 13: The average signal intensity shown in Figure 9 after applying the transmission correction.

To correct for this, a spectrum acquired in fixed mode under similar experimental conditions is used. The procedure is as follows: from the totality of time-resolved spectra acquired using snapshot mode, an average spectrum is constructed via simple averaging in the time direction of the counts in each binding energy bin. The spectrum acquired in fixed mode is then divided at each binding energy by the spectrum acquired in snapshot mode. This results in a positive[2] value at each binding energy bin. We call this the transmission function of the analyzer. Next, at each point in *time*, the spectra acquired in snapshot mode are multiplied by the transmission function to obtain a *transmission-corrected* spectrum.

An example of a corrected time-resolved spectrum, once more for the C 1s region, is shown in Figure 13.

[2]Because the spectrum acquired in fixed mode is a summation of counts in multiple bins, we expect is to be larger in count value than the spectrum acquired in snapshot mode on a per-binding-energy-bin basis.

2.3.3 Valence band spectrum aggregation

As discussed above, the pass energy setting on the electron analyzer controls the width of the binding energy window in which we detect photoelectrons. In order to obtain valence-band spectra, a lower incident photon energy is required. In our experiments, we use $E_\gamma = 70$ eV. Therefore, also a lower pass energy is required. We use $E_p = 60$ eV, which implies that the energy window is on the order of 6 eV.

As such, to obtain a complete valence band spectrum, we need to find some way to join together multiple snapshot spectra acquired at different binding energy ranges. I call this joining of spectra "stitching". To this end, I have implemented code in Python to facilitate spectrum stitching in a continuous fashion. In the overlap region between spectra, where there is data from two acquired snapshot spectra, I have decided to use a dimensionless constant instead of an average to combine the information from the two. This is exemplified in Figure 14. I introduce the dimensionless constant $\zeta \in [0, 1]$; ζ increases linearly from 0 to 1 in the overlap region. In the overlapping region, I take the stitched spectrum data in each binding energy B_e and at each time t to be $S_r(B_e, t) = S_{\text{right}}(1 - \zeta) + S_{\text{left}}(B_e, t)\zeta$.. Once this stitching step has been performed, together the previously-discussed energy calibration and transmission correction, the data is ready to be analyzed.

2.4 Overview of Fourier Transforms in the context of Fast Fourier Transform tr-APXPS

2.4.1 Review of Fourier Transforms on 1-dimensional signals

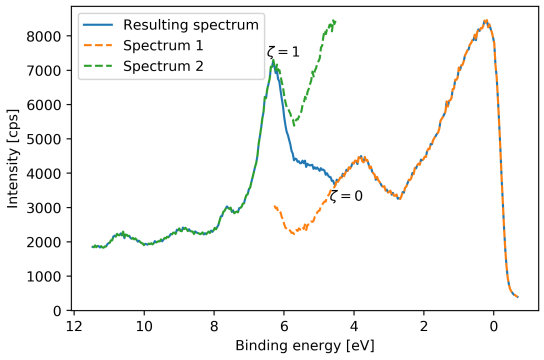

Figure 14: Figure showcasing the smooth transition from one spectrum to another in the overlap region.

As we have discussed in the previous sections, in a tr-APXPS experiment, the signal intensity - given by photoelectron count - is simultaneously sampled at several binding energies B_e (these are the signal channels) and with a given acquisition frequency. This acquisition frequency determines the time-point separation. The discrete Fourier Transform of the time-dependent intensity signal $s(B_e, t)$ is given by

$$S(B_e, f) = \sum_{k=0}^{N-1} s_k e^{-2i\pi fk/N} \tag{7}$$

where N is the total number of time-points used to sample the data. $S(B_e, f)$ is a complex quantity and therefore is endowed with both a magnitude and a phase. The magnitude is best regarded as an oscillation amplitude. Since the FT decomposes the signal into oscillating wave components with different frequencies, these terms may be regarded as the expansion coefficients in a basis composed of these waves.

We begin with demonstration of basic FT properties on a simulated dataset. Consider the following simulated signals in 4 binding energy signal channels, indexed by a fictitious binding energy B_m:

$$
\begin{aligned}
s(B_1, t) &= 4\cos(2\pi \cdot (10t)) + B_1 \\
s(B_2, t) &= 2\cos(2\pi \cdot (10t)) + B_2 \\
s(B_3, t) &= \cos(2\pi \cdot (10t) + \pi/4) + B_3 \\
s(B_4, t) &= \cos(2\pi \cdot (5t)) + B_4
\end{aligned}
$$

and notice that they we take a linear dependence on the binding energy, as well as a time-dependence. I take $B_m = m$ for simplicity. I show these signals in Figure 15 (a). In Figure 15 (b) the normalized oscillation amplitude (left scale, crosses) is shown together with the phase (right scale, filled points).

To understand the normalization of the oscillation amplitude, remember that the FT is given in frequency bins. This means that a natural normalization is to divide the "raw" FT oscillation amplitude values by the number of frequency bins.

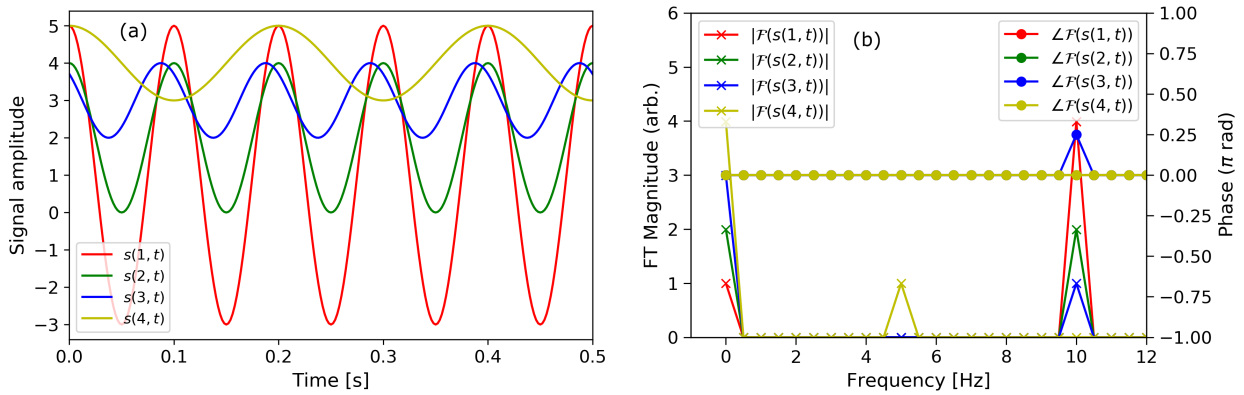

Figure 15: (a) Four purely sinusoidal signals, with different frequencies, offsets and phase shifts, and (b) The Fourier Transforms of the signals in (a), showing FFT magnitude (left scale) and denoised phase (right scale).

Looking at the normalized oscillation amplitudes of the FTs of the signals we have constructed, we see that they correspond to the original oscillations we have assigned to each of the signals. The zero-frequency components (i.e. the average of the signals) correspond to the static offsets of the signals (in our case, the B_m values) while the oscillation amplitudes are found in the expected frequency bins.

Now consider the phases of the signals. First, note that the algorithm used by NumPy to compute the FT takes a pure cosine signal as the zero-phase reference. Therefore, signals $s(B_{1,2,4}, t)$ show zero phase-shift, while signal $s(B_3, t)$ shows a phase-shift of $\pi/4$.

Note that it is important to consider the exact manner in which one calculates the FT phase. Indeed, the FT oscillation amplitudes in the frequency bins where no signal exists are not identically 0, but are instead values on the order of the floating point error due to machine precision (therefore $\approx 10^{-16}$), and so the phase oscillates wildly. A simple denoising technique, then, is simply to apply a window whereby the magnitudes below, say, a 1/1000th of the maximum magnitude are ignored. It is with this technique applied that I obtain the phase plots shown in Figure 16. I find out during

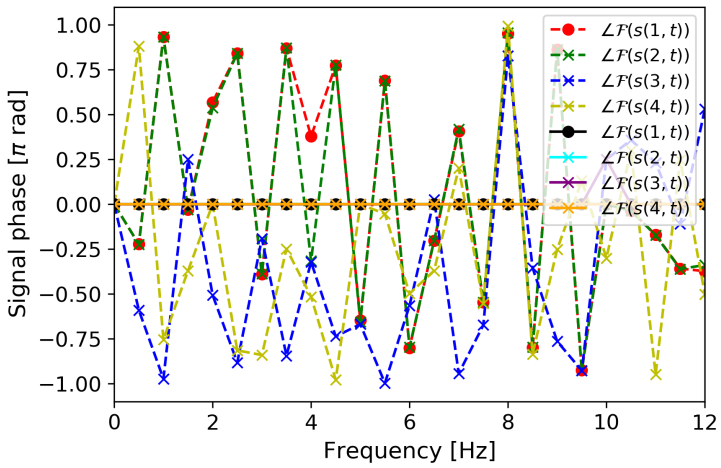

Figure 16: The FT phase spectra of the signals in Figure 15 (a) before (dashed lines) and after (solid lines) phase denoising.

the course of the work that phase information is very useful in determining, for example, the width of signal peaks, and so I do not use this denoising method in my work.

Since I am dealing with a purely real input signal, I am free to use the FFT algorithm implemented in the function `fft.rfft`, which computes the discrete Fourier transform only at positive frequencies [3].

The frequencies are computed simply by providing the number of time-points where the signal is sampled and the time-domain spacing thereof. The function `fft.rfftfreq` then generates the suitable positive sampling frequencies.

Finally, in processing the real experimental signal, our expectation will not actually be to see a purely sinusoidal signal. Therefore, higher frequency harmonics will be visible in the data. As such, we will not see a single peak in the Fourier Transform. Hence, it is instructive to look at a more complicated signal and its Fourier Transform.

Let us examine a sawtooth signal. Remember that a sawtooth signal with frequency f may be represented by the infinite series:

$$a\left(\frac{1}{2}-\frac{1}{\pi}\sum_{i=1}^{\infty}(-1)^i\frac{\sin(2\pi ift)}{k}\right) \tag{8}$$

and therefore we will have an infinite series of peaks in its Fourier transform. In principle, the largest peaks will occur at the fundamental frequency of the sawtooth wave and multiples thereof. In particular, we will take a sawtooth wave with frequency $f_s = 0.5236$ Hz. We show the wave and its Fourier Transform in Figures 17 (a) and (b), respectively.

It is possible to obtain the original signal, less the non-periodic noise in it, by inverting the Fourier Transformation, in a process called Inverse Fourier Transformation. The algorithm is called Inverse Fast Fourier Transformation (IFFT).

[3] This is adequate, since the value of the transform at the corresponding negative frequencies is in this case simply the hermitian conjugate of the transform value at the positive frequency values, which would give the same magnitude.

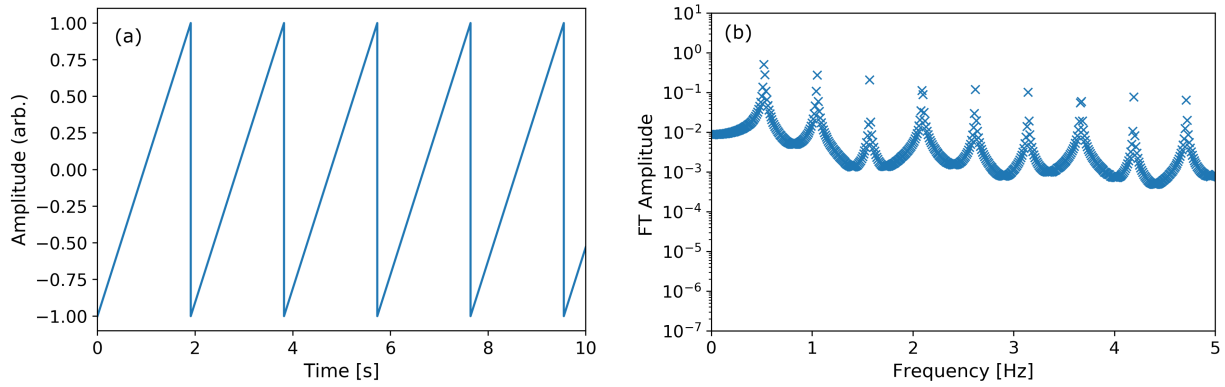

Figure 17: (a) Sawtooth wave with a frequency of $f_s = 0.5236$ Hz and (b) The Fourier Transform thereof.

Note that the Fourier Transform has non-zero components not only at multiples of the fundamental frequency of the wave, but also around it, and it is fundamental to remember that these non-zero component "bands" are crucial when attempting to reconstruct the original signal, and this is equally valid in this simulated example as in real data.

In Figure 18 (a) I show 3 different samplings (4, 20, and 30 points sampled around each peak, respectively) of the Fourier Transform and in (b) the signal reconstructions thereof.

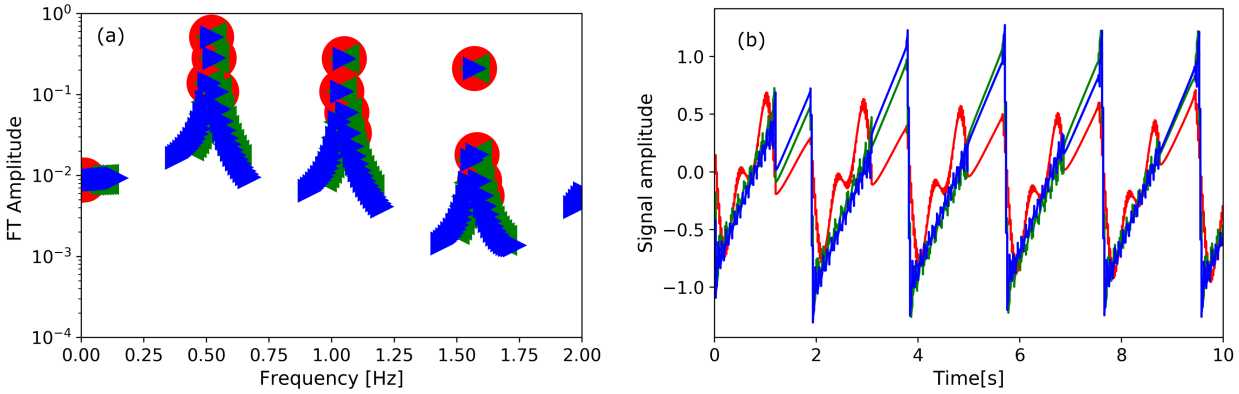

Figure 18: (a) Increasingly complete samplings of Figure 17 (b) and (b) the reconstructed signal therefrom.

This is meant to illustrate the importance of appropriately choosing data from which to reconstruct the Fourier Transform. Each point in the FT spectrum represents one additional wave to be added to the full signal reconstruction. Thus, for our particular example of the sawtooth wave, sampling only near the principal frequencies will reproduce the general periodicity of the sawtooth wave, but will not accurately reconstruct the amplitude and shape. The more additional peaks next to the principal harmonics we choose, the better the original waveform is reconstructed.

2.4.2 Application of FFTs to FT-APXPS data

As discussed in the data processing section, we obtain time-resolved spectra in the snapshot mode of the electron analyzer. To process them, we perform a Fourier transform in the time direction at each binding energy bin, thus creating a set of spectra we can analyze. An example of an FTed spectrum is shown in Figure 19 for C 1s data taken in a gas-pulsing experiment wherein the gas was pulsed at a frequency $f = 0.2$ Hz. The signal we see shows oscillation amplitude (given on a color scale) as a function of binding energy (x-axis) and frequency (y-axis). In the FTed image, there is signal visible at this (0.2 Hz) frequency and its multiplets. This is the basic spectrum we often will look at in the following sections.

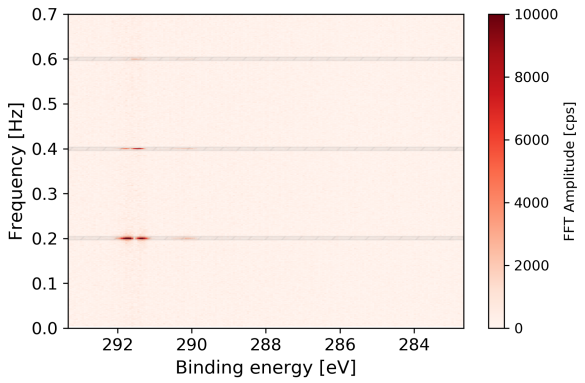

Figure 19: FFT Image of the time-resolved spectrum of C 1s taken in a gas-pulsing experiment with the 100 ms-wide gas pulses sent with frequency $f = 0.2$ Hz. The hatched areas are the parts of the FFT used to reconstruct the signal.

On the basis of this spectrum, both the phase as well as the magnitude of the Fourier transform of the time-resolved signal may be obtained for each binding energy and at each frequency. Therefore, it is useful in providing information regarding how strongly the core- and valence-band-level peaks found in the average signal obtained from the time-resolved spectrum oscillate. Furthermore, it provides information regarding whether they oscillate simultaneously or with some finite phase difference, and, crucially, which peaks oscillate in-phase and out-of-phase, respectively.

This ultimately enables the in-depth study of the surface dynamics which occur during the catalytic oxidation of CO, and, finally, with a mask applied onto the FTed image to filter out irrelevant noise, it also enables us to reconstruct the original peak signal in a manner entirely analogous at each binding energy bin to a reconstruction in the one-dimensional case discussed previously.

An example proves to be illuminating. Consider the case of the C 1s spectrum. Now, from the FT image, I select using a mask the areas in the hatched region on the image in Figure 19 and use them to reconstruct the original signal. In Figure 20 is the original time-resolved spectrum alongside the reconstructed time-resolved spectrum, zoomed into an arbitrary region 3 gas-pulse cycles long (15 seconds at a period $T = 5$ s).

Even when adding the background (the absolute value of the 0 frequency component of the Fourier transform), the difference in quality between the spectra is striking. The reconstructed spectrum shows a much clearer signal.

2.5 Correction for effects due to the periodic nature of the gas pulses

As outlined in previous sections, the present work deals with CO oxidation over Pt(111) in the presence of periodic gas pulses. Since the raw intensity of the spectra under consideration is affected by the travel of the photoelectrons through the gas phase just above the sample, the variation in gas pressure induced by the periodic pulsing of gas above the sample will result in an oscillation in the spectrum intensity at the same frequency as that of the gas pulsing operation.

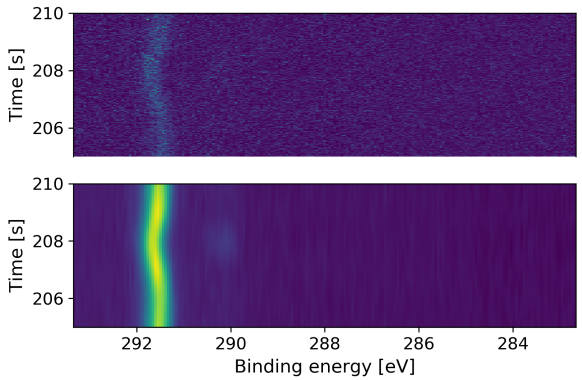

Figure 20: Comparison of the (top) original time-resolved spectrum of C1s used to obtain the FFT image in Figure 19 and the (bottom) time-resolved spectrum obtained by inverting the FFT signal in the hatched regions shown in Figure 19 and adding the constant background contained in the 0 frequency component thereof.

we are interested in.

When examining the surface position, secondary electron emission will be detected in the form of a background signal around the core-level peaks in both snapshot and fixed mode. Since in fixed mode these effects should have been averaged out, we can again use the fixed mode spectra in areas with no signal peaks to normalize our data. Where there is only secondary (bulk) electron emission, we can assume that this emission should not vary with the surface structural changes.

Therefore, at each point in time in the snapshot, we normalize by using the ratio between the integrated intensity in snapshot mode and the integrated intensity in the fixed spectrum spectrum, computed in a region with only secondary emission.

Consider how this affects the interpretation of the data. We have a reaction which in principle is kick-started by the introduction of a gas-train pulse. The partial pressure of the gases above the sample (as well as the overall composition) changes with the introduction of this pulse, both due to the additional gas in the pulse, as well as due to the increase in CO_2 production which accompanies it. Therefore, the gas-phase attenuation of photoelectrons increases (and then decreases) accordingly. Worse still, this attenuation variation will have the same frequency as that of the gas pulses themselves, which in turn means that the change in signal due to this will directly confound the change in signal due to geometric and electronic structural changes on the surface. Therefore, it is important to remove this effect in order to facilitate an accurate evaluation of the physical effects

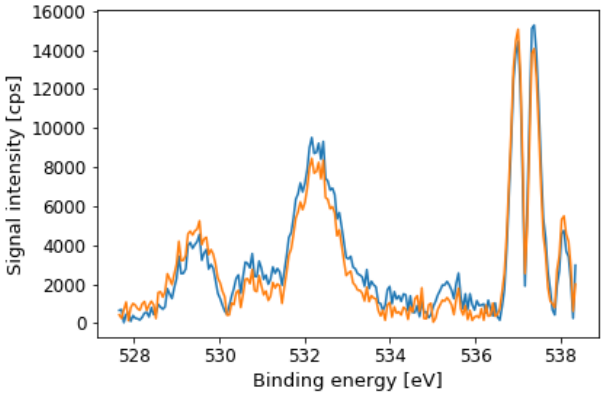

Figure 21: The FT magnitude of the recorded O 1s (s) spectrum before (orange) and after (blue) correcting for the time-varying attenuation in the gas phase.

I do note that this correction should only be applied to those spectra examined near the sample surface, as the gas phase itself is of course affected in composition by the introduction of the gas pulses, and in that case the variation in spectral intensity is itself a result we are interested in.

2.5.1 The FFT-XPS analysis package

All code used in the development of this work has been written in Python. The approach used was class-based in order to provide a convenient workflow. The original FT-APXPS functionality of the module was based on code discussed with my supervisor Jan Knudsen and implemented by him in the spectrum analysis program Igor Pro. We discussed the mathematical principles involved,

common pitfalls, and a general overview of what his code does, with demonstrations. The technical implementation in Python is fully my own work. The spectrum stitching functionality was conceived and implemented by me independently.

3 Results

3.1 Core-level XPS data in the gas phase

3.1.1 C 1s core-level spectra in the gas phase

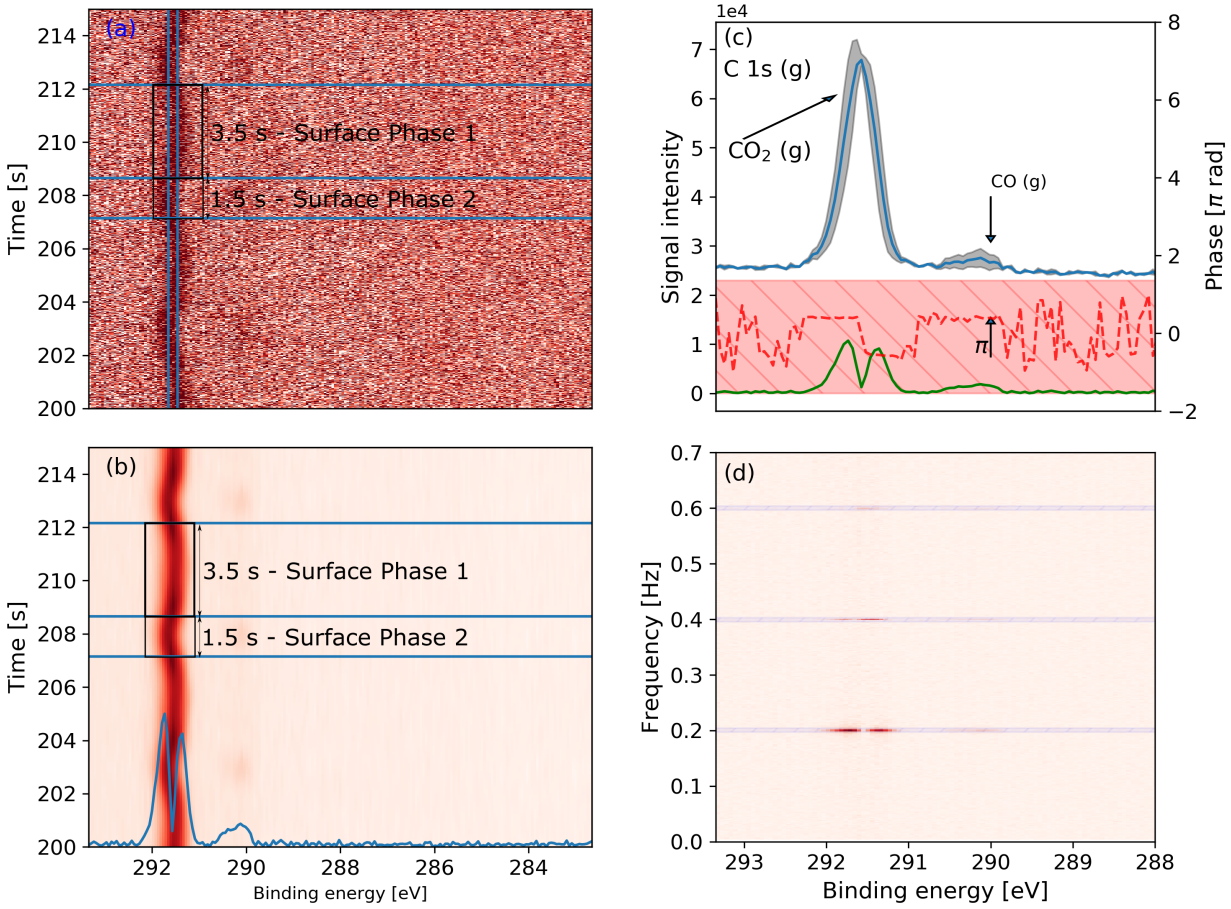

Figure 22: (a) Figure showing a 15 s long image of the C 1s gas phase spectra, (b) the reconstructed image of the same (same 15 s snapshot reconstructed using entire dataset), with (blue) overlaid fundamental-frequency FT magnitude. (c) the (blue) average signal of the time-resolved C 1s spectrum, (green) the FT signal at the fundamental frequency $f_0 = 0.2$ Hz, (gray) the resulting oscillation in the average signal, and (dashed red) the oscillation phase in terms of π radians. The hatched red region corresponds to background secondary electron emission. (d) shows the FT image of (a) along with the selected mask for obtaining the reconstructed spectrum in (b).

First I show the results corresponding to the C 1s spectra measured in the gas phase, at a distance of 0.3 mm above the sample surface. The sample temperature is $T = 565$ K. CO is, as specified earlier, pulsed at a frequency of $f_{\mathrm{CO}} = 0.2$ Hz on top of a constant 3.5 sccm background flow of O_2.

The photon energy used to acquire the spectrum and all subsequent C 1s spectra is $h\nu = 450$ eV, with a pass energy $E_p = 100$ eV.

In Figure 22 I show (a) a 15-second long snapshot of the C 1s (g) time-resolved spectra, (b) the reconstructed time-resolved spectrum obtained from inverse Fourier Transforming a selected region of the Fourier Transform of the original time-resolved spectrum. Overlaid over the reconstructed image is (blue) the FT magnitude of measured at the fundamental frequency $f = 0.2$ Hz.

Figure 22 (c) shows (blue) the average signal from the time-resolved spectrum, (grey shadow) the oscillation amplitude as resulting from the FT amplitude, (green) the FT amplitude and (red) the phase of the oscillations. In (d) the FT transform of the entire time-resolved spectrum shown in (a), along with the areas used to obtain the reconstruction shown in (b), are highlighted in hatched white shadowing.

The workflow when working with the spectra is (a)→(d)→(c)→(b), that is, the time-resolved data gets Fourier Transformed ((a)→(d)), then, by selecting the area in the Fourier transform corresponding to all information in the 0.2 Hz bin at all binding energies, a line scan in the binding energy direction at this frequency is obtained, ((d)→(c)), and finally, all relevant FT data is used to obtain a reconstruction of the original signal with the noise (and background) filtered out ((d)→(b)). A summarizing drawing of the workflow of FT-APXPS is shown in Figure 23

Now we return to the interpretation of Figure 22. From the figure, together with the information provided in the time-resolved spectrum, we get a first hint at the progression of the catalytic reaction.

On the basis of the work of Knudsen et al. on CO oxidation over Pd[7], I assign the peak at 291.5 eV to CO_2 (g), and the peak at 290.2 eV to CO (g). In the CO_2 signal, the large feature present in the average signal becomes split into two oscillating components. The split between the two oscillating peaks in the FT data is 0.4 eV (one peak at 291.75 eV and the other at 291.35 eV). This is caused by a work function shift, as explained in Eq. 6. If we were to look only at the apparent shift of the "center" of the average signal, we would find a shift of about 0.2 eV, which is lower than the shift in the FT peaks. This is because the peak of the "average" XPS signal is closer to one of the FT peaks. The duration of the work function shift is shown using black squares in Figure 22, and it is roughly 1.5 s. Therefore, the duration of the other state is 3.5 s (the entire cycle is 5 s). From this, we must conclude that at least part of the surface atoms oscillate between two structural configurations, or *surface phases*. I assign to the 1.5 s long state the name Surface Phase 2, and to the 3.5 s long state the name Surface Phase 1. I note that Surface Phase 2 is associated with a work function shift of spectral features towards higher binding energies relative to the position of the feature in the time-average spectrum, while Surface Phase 1 is associated with a shift towards lower binding energies relative to the same. We are satisfied that the two components oscillate in anti-phase thanks to the phase signal associated with the Fourier Transform, whence it is clear that there is a phase difference of π between the two signals.

It is also worth discussing the relative size of the oscillating components to the average signal. Integrating the area under the average signal peak, we get $I = 46.9 \cdot 10^4$ cps. Meanwhile, the higher oscillating peak, at higher binding energy, integrates to $I_h = 3.3 \cdot 10^4$ cps, while the lower peak integrates to $I_l = 2.3 \cdot 10^4$ cps, meaning that we gain the following information: the shift in CO_2 production due to the change in surface phase accounts varies between 5% and 7%. This means that we deal with a minority oscillation in CO_2 production, with most of the production rate being constant.

This interpretation is consistent with the expected mechanism of the CO oxidation reaction[25].

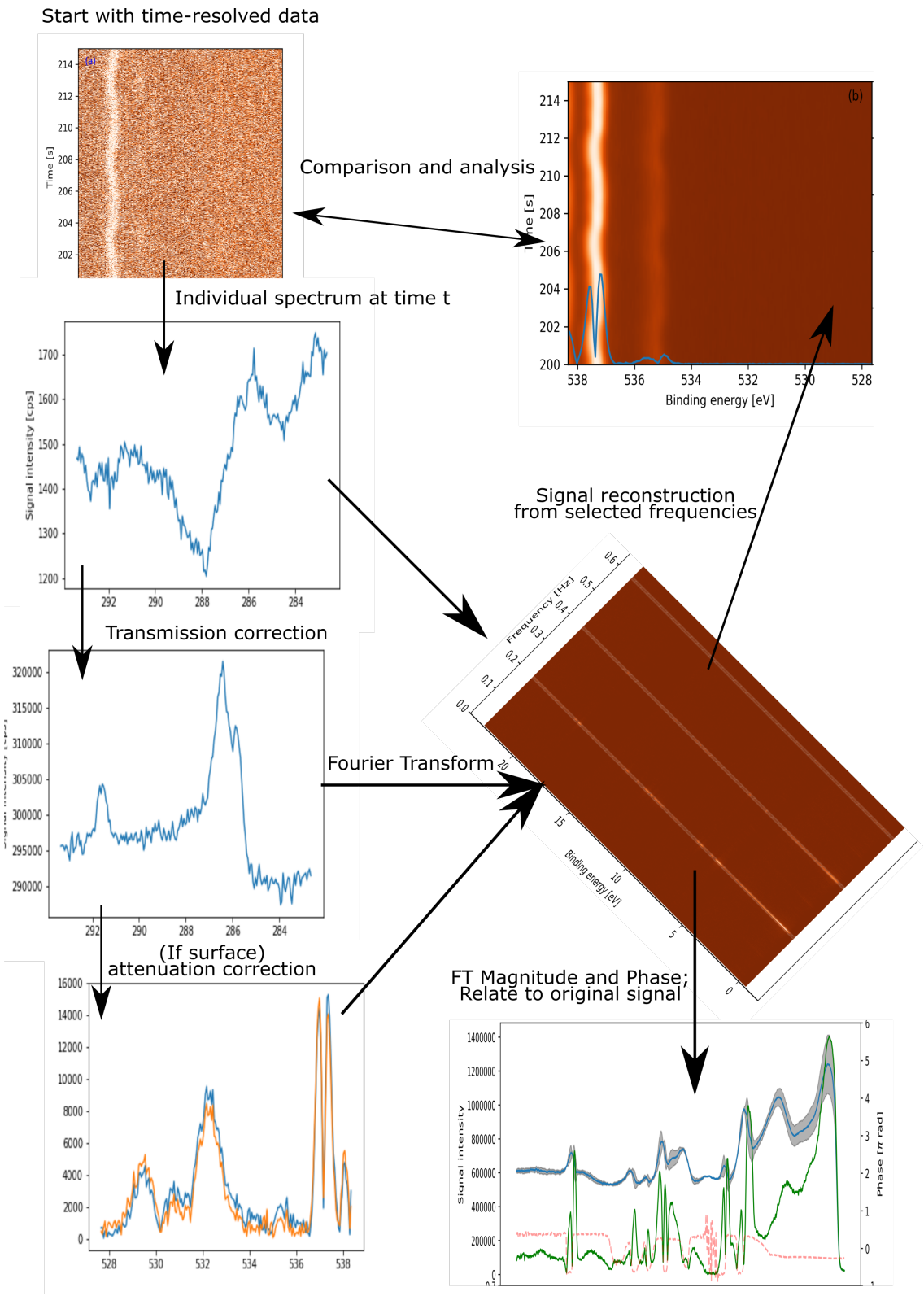

Figure 23: The workflow of FT-APXPS and FT-APUPS in this work. Not shown are further quantitative analyses which can be performed. These are discussed in the outlook.

Once we send a CO gas pulse into the experimental cell, the sample oscillates in and out of the CO mass transfer limit. CO_2 is produced all throughout the process, while CO dissipates after the pulse is introduced. This is also consistent with the time-resolved image (the easiest way to see this is in Figure 22 (b)). When the CO pulse is introduced, signal appears spread around 290.2 eV, consistent with our assignment of this peak to CO. This increases the production of CO_2 and triggers the shift in the CO_2 signal, which is clearly visible in the time-resolved spectrum as well.

To summarize, what we can so far conclude from the data is the following: there is a minority oscillation on the surface between two surface phases. There is an "apparent" work function shift of 0.2 eV between the location of the peak associated with CO_2 in the time-average XPS signal in Surface Phase 1 and Surface Phase 2. Thanks to the ability of FT-APXPS to selectively probe the surface and identify minority oscillations (high sensitivity), I am able to determine that the real work function shift is 0.4 eV, in line with literature results.[15]

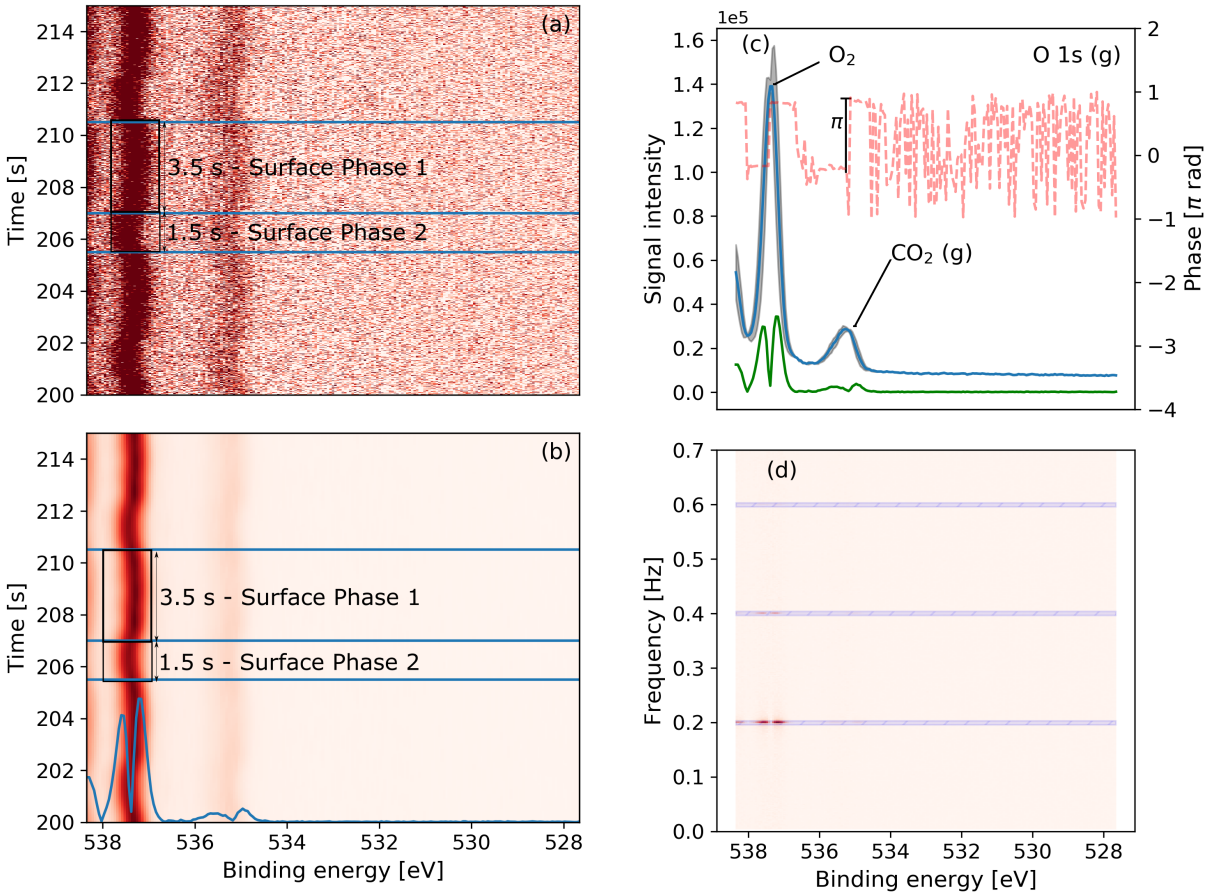

Figure 24: (a) the time-resolved spectrum of the O 1s (g) core level; (b) the reconstruction thereof via inverse Fourier Transform. Overlaid is (blue) the FT magnitude at the fundamental frequency. (c) the (blue) average signal of the time-resolved O 1s spectrum, (green) the FT signal at the fundamental frequency $f_0 = 0.2$ Hz, (gray) the resulting oscillation in the average signal, and (dashed red) the oscillation phase in terms of π radians. The hatched region corresponds to background secondary electron emission. (d) The FT image of (a) along with the selected mask for obtaining the reconstructed spectrum in (b) of the same.

We proceed to examine the other spectra in order to try and discern what specific structures char-

acterize the surface in each of the two phases hypothesized above.

3.1.2 O 1s core-level spectra in the gas phase

We now proceed with an examination of the O 1s gas phase spectra obtained in the same conditions as those of section 3.1.1.

We proceed to examine the results in a similar manner as before. Therefore, in Figure 24 I show an image (a) of the time-resolved spectrum of the O 1s core-level photoelectron, with (b) the reconstruction thereof from the fundamental frequency and first three harmonics of its FT signal, isolated such that only relevant parts of the signal are visible. In (c) I show the average signal (blue) together with the oscillation (shaded gray) in it, and the FT magnitude (green) at the fundamental frequency $f = 0.2$ Hz and FT phase (dashed red). The FT image is shown in (d), with the areas used for the above-mentioned reconstruction hatched.

The large feature at 537.4 eV in the average signal can be attributed to molecular Oxygen in the gas phase above the sample. This is supported by the peak's deconvolution into two peaks in the FT magnitude image and by the oscillation of these in anti-phase. Do note that our binding energy window is not enough to capture the Oxygen doublet, but that it is partly visible at the high binding energy edge of the spectrum (see in particular subfigure (b)) during Surface Phase 2. As before, the duration of Surface Phase 2 is 1.5 s and that of Surface Phase 1 is 3.5 s.

Indeed, comparing with the C 1s (g) spectrum of the previous section, the separation between the FT-deconvoluted peaks of the O_2 feature is 0.4 eV, consistent with the work-function shift observed in the C 1s (g) spectrum features attributed to CO_2. Relevantly, previous work by Johansson et al. [15] has also confirmed a work function shift of 0.4 eV when transitioning from a CO-covered surface to an oxygen-covered surface in the case of CO oxidation over Pt(111).

Consider now Figure 25, where the peaks of features are marked by vertical lines and the phase (dashed black) is overlaid. The (blue) lines at 537.58 and 537.18 eV I attribute directly to molecular Oxygen components above surface patches with two different work function shifts, as described above. Consider now the peaked feature at 535.4 eV (red). A shift of 0.4 eV would result in the (red) peak at 535 eV. These two features are rather broad, so peak positioning can be regarded as quite subjective, however if we do accept this assignment, then these two peaks can be seen as the deconvolution of the CO_2 peak shown in the average signal. To strengthen this argument, the two peaks oscillate anti-phase, which would be consistent with this assumption.

One confounding factor yet remains: In the assignment performed for the C 1s (g) spectra, we saw that the CO_2 FT peak with the highest binding energy (Surface Phase 2) had the largest oscillation amplitude (both peak amplitude and integrated value). The work function shift should occur in the same direction in the O 1s data as well.

At first inspection, it appears as though this is inverted here, since the largest CO_2 oscillation amplitude appears at the lowest binding energy. The explanation is that since the deconvoluted CO_2 features are broader, the integral of the signal under the peaks must be employed instead. We use the blue and red-hatched regions for in Figure 25 as integration regions in the binding-energy direction. The integral in the blue region is $I_2 = 1452$ and the one in the red region is $I_1 = 1206$, in keeping in line with what we would expect from the C 1s (g) spectrum, as the integrals in the C 1s (g) spectrum, done in the corresponding regions for the FT features assigned to CO_2 are $I_2' = 3352$ and $I_1' = 2410$. It is also worth it to answer the question of why there is an unevenness in the integral values to begin with. The higher binding energy FT peak (in Surface Phase 2) corresponds

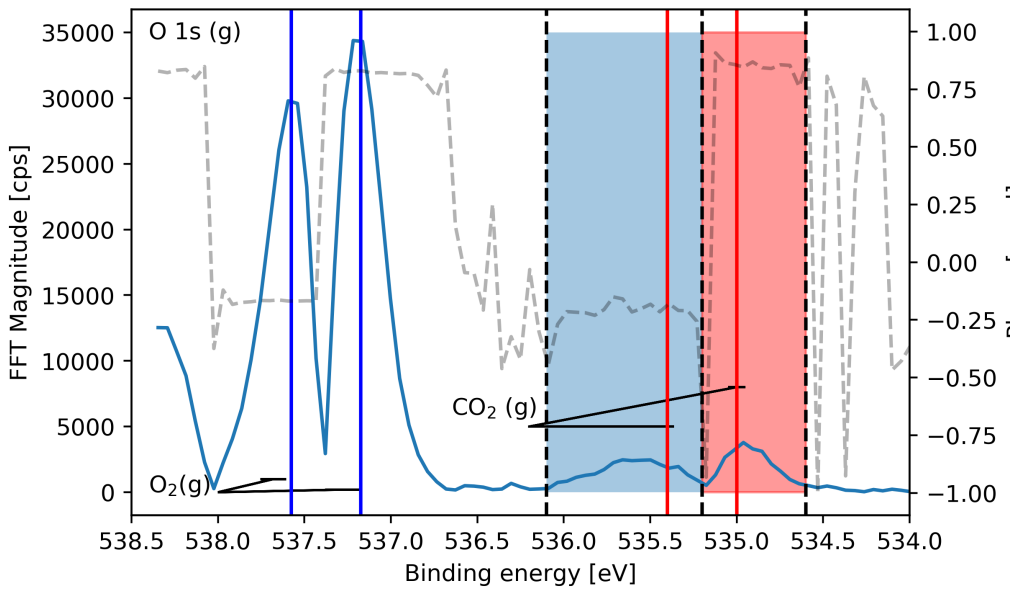

Figure 25: Peak assignment in the FT magnitude image for the O 1s (g) spectrum

to a state just after the introduction of the CO pulse. Therefore, the CO_2 production is increasing, so it makes sense that in this state we have a higher CO_2 FT signal.

Now we turn our attention to surface spectra.

3.2 Core-level spectra in the surface position

We now proceed with a discussion of the C 1s, O 1s and Pt 4f surface spectra. Now, in contrast to the previous results, we also expect a significant contribution from chemical species on the surface of the sample.

3.2.1 C 1s surface core-level spectra

The spectra were recorded under the same pulsing conditions as the gas phase spectra. The temperature was different, namely $T = 543$ K. Figure 26 shows the (a) time-resolved and (b) reconstructed time-resolved C 1s spectra via inverse Fourier Transform, with the (blue) FT magnitude. The usefulness of the signal reconstruction technique is evident in this case as the signal is much more easily discernible than in the raw time-resolved spectrum. Because we see no clear gas-phase species in the spectrum, it is not possible to directly identify the duration of Surface Phases 1 and 2.

Further, in (c) I show the (blue) oscillation signal with the (green) FT magnitude and (red dashed) phase at the fundamental frequency. (d) shows the FT image of (a) and the signal used to obtain the reconstruction in (b) is hatched.

We proceed with the interpretation in (c). We know from the work of Björneholm [14] et al. that there are two possible adsorption sites for CO on Pt(111). In particular, one of the likely structures is a c(4×2) or c($5 \times \sqrt{3}$) structure with the CO molecules adsorbed in on-top and bridge sites, with corresponding signal in the C 1s spectrum at 286.7 eV (blue line) and 286.0 eV (red line), respectively

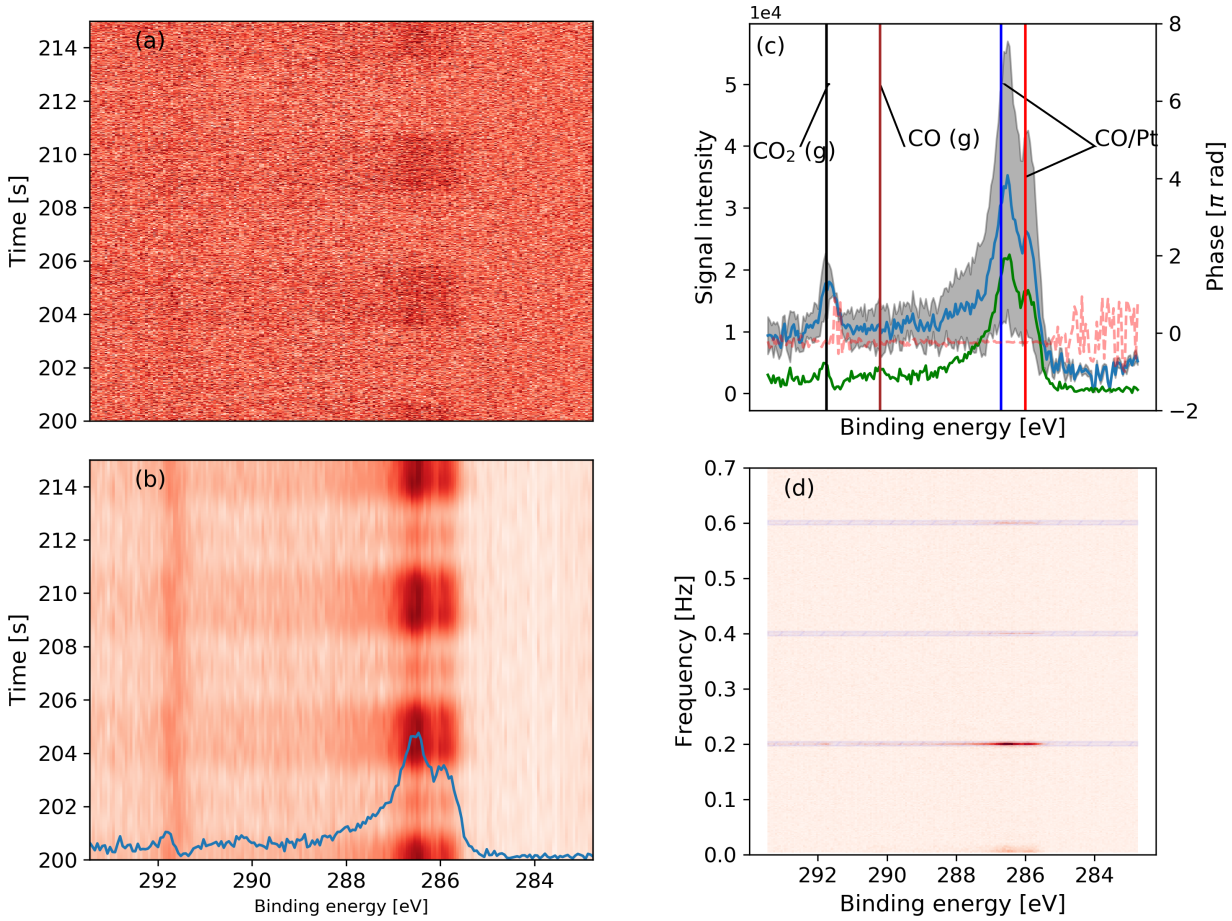

Figure 26: (a) shows the time-resolved spectrum of C 1s in the surface position. (b) shows the reconstructed image of (a) using the inverse Fourier transform, together with the FT magnitude (blue) at $f = 0.2$ Hz. (c) shows the average signal in the spectrum (blue), with the oscillation in it (gray shading), together with the FT magnitude (blue) and phase (red dashed). (d) shows the FT image of (a) with the selected frequency cut-outs used to obtain the image in (b).

We can reasonably contend that these correspond to the features found in our spectrum. In favour of this assignment is also the fact that the peaks oscillate in-phase (as would be expected if both of these features are due to a single type of CO/Pt(111) structure) and that they do not show up in the corresponding C 1s (g) spectrum, meaning that they have to be due to surface species. Furthermore, as this is a C 1s spectrum, there can be no confounding contribution from O_2 (g).

It is worth examining the evidence for the nature of the CO structures on Pt(111) more closely. It need not necessarily be the case that only the coverage of the structure oscillates, but it could also be that different, less or more dense structures do appear. However, the two CO/Pt peaks in Figure 26 (c) oscillate in-phase, which means that both the bridge and atop sites are being occupied or vacated simultaneously, so it cannot be the case that we transit from the more dense structure to the less dense c(4×4) structure which only contains atop sites. In light of the relative intensities of the bridge and atop sites, I find it likeliest that the structure is the c($5 \times \sqrt{3}$) structure. I find no evidence for a transition between the two denser structures (c($5 \times \sqrt{3} \leftrightarrow$ c(4×2))) as the relative intensities of the peaks in the FFT magnitude are identical to the relative intensities in the average

data.

At 291.5 eV, a small feature (black line) is visible and, due to previous arguments brought forth when discussing the C 1s (g) data, I assign this to CO_2 (g). Arguably, a feature is *also* visible in the FFT data at 290.2 eV (brown line). This corresponds to CO (g), also as discussed in the previous section.

3.2.2 O 1s surface core-level spectra

Now we examine the O 1s surface spectrum. The pulsing conditions are the same as in the other measurements, and the temperature is $T = 543$ K. In Figure 27 I show (a) a section of the time-resolved spectra of the O 1s energy level. (b) shows, as before, the reconstructed signal from the inverse Fourrier transform alongside (blue) the FT magnitude.

In the case of the O 1s surface spectrum, the signal from the Fourier transform magnitude is comparatively weak due to the presence of a very large secondary bulk electron emission signal.

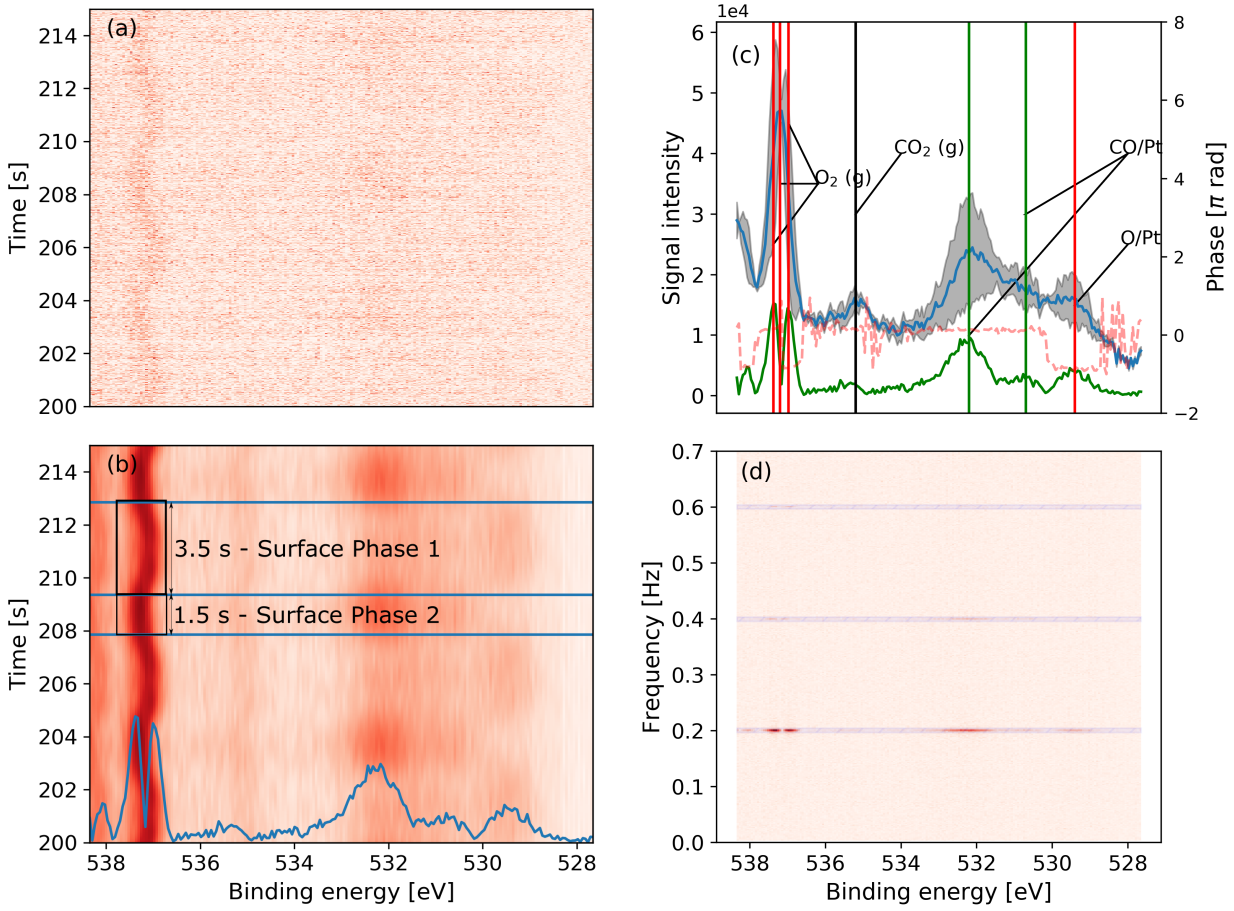

Figure 27: (a) shows the time-resolved spectrum of O 1s in the surface position. (b) shows the reconstructed image of (a) using the inverse Fourier transform, together with (blue) the FT magnitude at $f = 0.2$ Hz. (c) shows the average signal in the spectrum, with the oscillation in it, together with the FT magnitude and phase shown in (b). (d) shows the FT image of (a) with the selected frequency cut-outs used to obtain the image in (b).

Examining (c) proves instructive. It shows (blue) the average signal with removed secondary electron emission (flat background subtraction) with (gray shading) the oscillation therein obtained from the (green) FT magnitude and (red dashed) phase at the fundamental $f = 0.2$ Hz. In the region between $E_b = 528$ and $E_b = 533$ eV, there is a broad feature in both the average signal and the Fourier transform, with the feature at 529.5 eV oscillating in anti-phase with the two features at 531 eV and 532.3 eV. We can be sure that the signal in this region is due to chemical species adsorbed on the surface because it does not show up in the O 1s (g) signal. The results of Schnadt et al.[25] and Björneholm et al. [14] are useful in interpreting this. Essentially, we are seeing a convolution of peaks due to atomic oxygen adsorbed on the surface (the feature (red) at 529.4 eV) and due to CO adsorbed on the surface (the features (green) at 530.7 and 532.2 eV, which are comparable to Björneholm's proposed values of 531 eV and 532.7 eV, respectively, for CO/Pt(111)c(4x2)/c($5 \times \sqrt{3}$), as discussed in the previous section). The fact that they oscillate in anti-phase makes sense in context. As more CO adsorbs onto the surface, the oxygen coverage decreases.

Finally, the large feature (red) at 537.2 eV in the average signal spectrum deconvolutes into two features (red) at 537.38 and 536.98 eV, which confirms that this is a gas-phase peak detected above the sample surface. This I attribute to molecular O_2. From this, and from the O 1s (g) spectra presented in the previous section, it is important to note that we see a strong oxygen signal present at all times, which means that oxygen gas exists above the sample at all times during the reaction. This is in contrast to, for example, the oxygen-limited condition that is possible as per Knudsen et al. [7].

This is supported by the existence of the feature (black) at 535.2 eV, which I attribute to CO_2 in the gas phase right above the sample surface. This is a peak which could be mistaken for noise were in not for the coherent phase signal associated with it. In this way we use the existence of phase information to confirm the existence of a feature in the FT magnitude and average signal spectra. Additionally, the phase itself is the same as that of the features attributed to CO, which makes sense for the reaction under examination, as the more CO adsorbs onto the surface, the more CO_2 signal will also be observed.

Because there is a gas-phase species clearly visible, it is easier to identify the extent of Surface Phases 1 and 2 in Figure 27 (b). In terms of the gas-phase shift, they keep their respective durations. However, the signatures of CO/Pt seem to extent for a bit longer. Moreover, in the reconstructed spectrum it is clear that CO/Pt signatures appear during the time of peak signal for O/Pt, which suggests the partial coexistence of these two surface structures.

3.2.3 Pt 4f surface spectra

The final surface spectrum we consider is the Pt 4f spectrum. As before, we look at (Figure 28 (a)) the time-resolved spectrum in a selected region, the (b) associated reconstructed time-resolved spectrum along with the (blue) FT Magnitude. We also look at (c) the (blue) average signal in the spectrum, its (gray shading) oscillation and (green) FT magnitude and (red dashed) phase at the fundamental frequency. The FT magnitude has been adjusted by a factor of 12 upwards in order for its features to be visible. (d) shows as previously the FT image of (a) and the areas of it (hatched) used to obtain the reconstruction in (b).

We see that the average signal displays two large features centred on 71 eV and 74.5 eV, respectively. This is the Pt 4f spin-orbit doublet splitting. The rightmost peak corresponds to the $4f_{\frac{7}{2}}$ component while the leftmost peak corresponds to the $4f_{\frac{5}{2}}$ component.

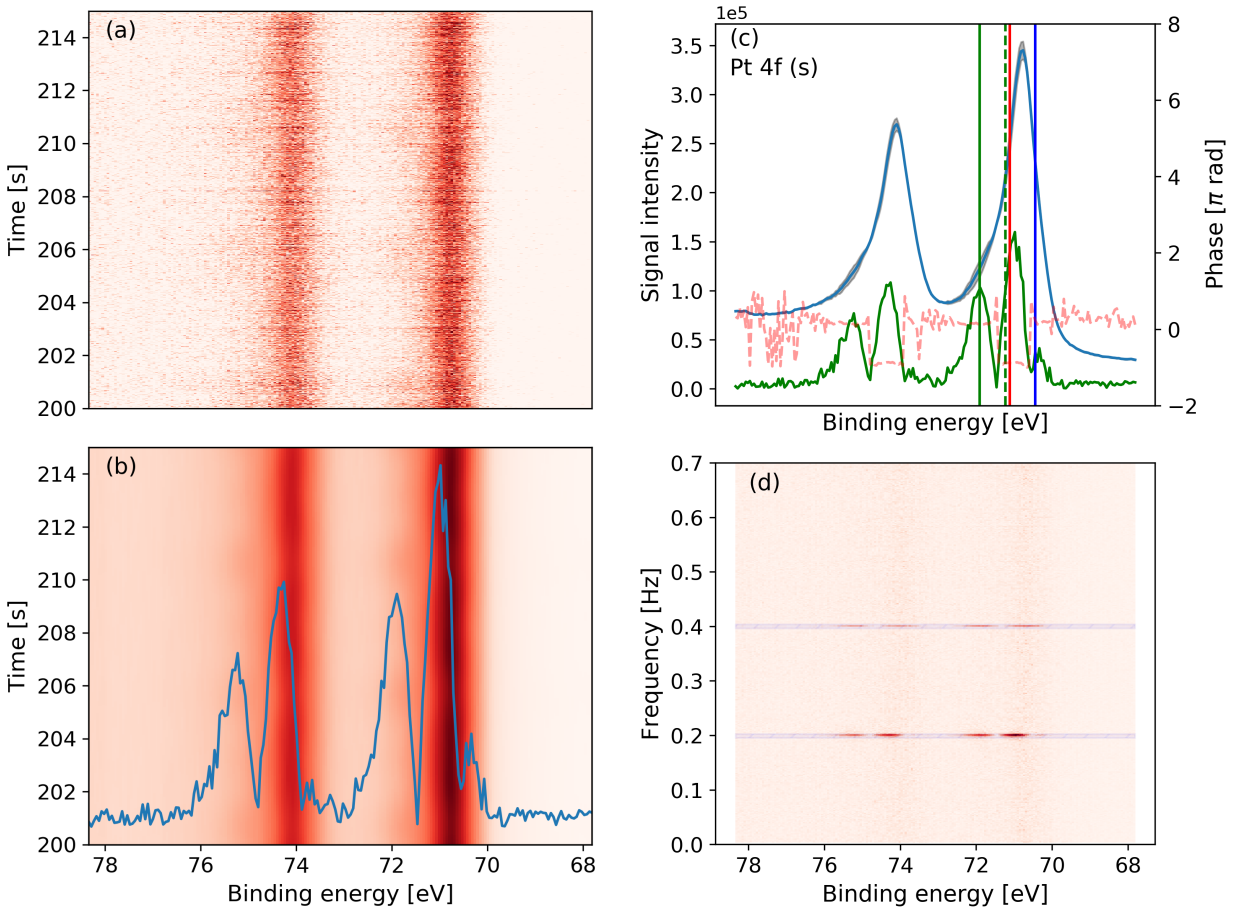

Figure 28: (a) the time-resolved spectrum of the Pt 4f spectrum in surface position. (b) shows the reconstructed spectrum using the inverse FT and shows overlaid the FT magnitude at $f = 0.2$ Hz. (c) shows the average signal in the spectrum along with the oscillation in it, with the FT magnitude and phase shown at $f = 0.2$ Hz. (d) shows the FT image of (a) with the areas of it which are used to obtain the reconstruction in (b).

Following again the results of Björneholm et al., we attribute (measured on own data) the feature at 71.91 eV (green line) to CO/Pt(111) adsorbed onto an on-top site, and the feature at 71.12 eV (red line) O/Pt adsorbed onto a hollow site. The green dashed line shows the expected position of the CO/Pt adsorbed onto a bridge site, but this cannot be distinguished from the Oxygen signal, if indeed it is there. The reason for this is that the oxygen signal probably dominates. Consider the case of two signals which are exactly out-of-phase (as we would expect the O/Pt-hollow and CO/Pt-bridge signals to be). The phase of the signal resulting from their addition will be the phase of the larger (in magnitude) signal. This suggests that the oxygen signal is larger than the CO/Pt-bridge signal.

Finally, the feature at 70.45 eV (blue line; compare to Björneholm et al.'s suggested 70.5 eV) corresponds, then, to clean Pt(111). It is interesting to notice that some surface atoms do actually become clean during the oxidation reaction. The growth of the clean Pt signal corresponds to a decrease in the signal due to adsorbed oxygen. One explanation for this dynamic is that as the CO

molecules react with adsorbed oxygen to form CO_2, the rate of reaction and desorption is higher than the rate at which additional O atoms can adsorb onto the surface, thereby leaving some Pt atoms free.

Let us now obtain an estimate of the proportion of platinum atoms which undergo a phase transition during the oxidation reaction. We can get a rough estimate as follows: given that the photon energy use to obtain the Pt 4f spectra is $h\nu = 200$ eV and that the $4f_{\frac{7}{2}}$ doublet is located at roughly 71 eV, the kinetic energy of the photoelectron reaching the analyzer is (roughly) 130 eV. At 130 eV, in Pt, the mean free path of the electron is on the order of 4 Å[29]. In Pt(111), which is endowed with an FCC structure, the interlayer distance is around 2.3 Å, which means that we probe at most 2 atomic layers deep into the sample. Therefore, around half the large average XPS signal belongs to the surface atoms. Integrating the area under the average signal corresponding to the extent of the FT peaks in the binding energy direction, and dividing by 2, we obtain $I_{\text{avg}}/2 \approx 254000$ cps. Integrating the area under the FT peaks, we obtain a total oscillation of $I_{\text{FFT}} \approx 14000$ cps. This means that only around 2.8% of the surface atoms actually oscillate during the catalytic reaction. Additionally, it is worth mentioning that the two peaks oscillating in phase (blue + green lines) add up in their integrate area to the peak they oscillate in anti-phase to (red). This means that the total oscillation amplitude is conserved. In other words, a constant percentage of the surface oscillates, which is as we would expect.

3.3 Valence band spectra

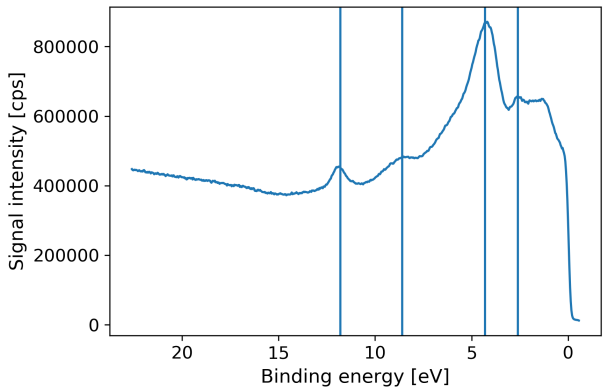

Figure 29: UPS spectrum of clean Pt(111) obtained under UHV conditions.

We now proceed to examine the valence band spectra, which we have measured under three experimental regimes: gas phase, surface position, and surface position with a clean surface under UHV conditions. The pulsing conditions are the same as for the core level spectra. The Temperature is $T = 570.15$ K for the gas phase spectra and $T = 553 - 558$ K for the surface spectra. We first look at the spectra of the clean sample.

3.3.1 Valence band spectra under UHV conditions and with pure gas

First, we briefly look at the average signal in the valence band spectrum when no gas is being pulsed into the cell and no background flow is present. This, then, is the clean Pt valence-band spectrum obtained under UHV conditions and is shown in Figure 29. Since the chamber is in imperfect UHV conditions, we actually expect the surface not to be clean, but rather to be CO-covered. I identify 4 features in this spectrum, at 11.8 eV, 8.6 eV, 4.3 eV and 2.6 eV (marked by vertical lines).

To aid in discerning which peaks belong to each chemical species, we also use spectra taken with only CO and only O in the sample chamber, respectively. This is shown in Figure 30.

The green spectrum is the spectrum measured in a pure CO atmosphere, shifted by 0.45 eV. The original unshifted spectrum is shown in dashed blue. In particular, this is evident around the 0 eV binding energy region. The measured CO spectrum is misaligned with the average measured

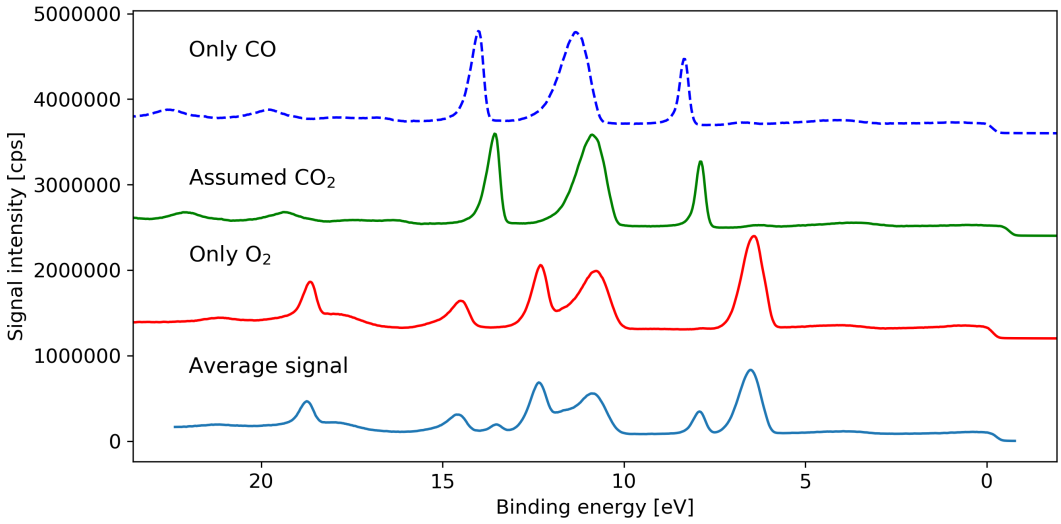

Figure 30: The valence band spectrum of (blue) the average gas-phase signal during the oxidation of CO, (green) only CO being pumped at a constant rate into the cell with a -0.45 eV shift, (red) only O being pumped at a constant rate into the cell. (dashed blue) the original unshifted spectrum recorded in pure CO. Due to considerations discussed in the text, we attribute the green spectrum to CO_2 and the dashed blue spectrum to CO. Spectra have been shifted up for clarity.

spectrum during the reaction. Therefore, the peaks in the actual measured average spectrum which align with the shifted measured CO spectrum can actually can be argued to correspond to the CO_2 valence band spectra. The signature "three-peak" appearance of the spectrum appears in both the CO and CO_2 valence-band spectrum. [30][31]. The reason I ascribe the spectral features to CO_2 is that we have learned from examination of the core-level spectra that we ought to expect significantly higher signal intensity from CO_2 than from CO in the gas phase. Therefore, in Figure 30, I attribute the red spectrum to O_2 and the green spectrum to CO_2, rather than CO. The original CO spectrum's middle peak can be argued to contribute to the shoulder in the average signal around 11 eV.

3.3.2 UPS spectra during CO oxidation

Now we look at the valence band spectrum in the gas phase above the sample. The familiar presentation form of the core level spectra is still useful in this case, especially as it renders a direct comparison of the effectiveness of FFT-APUPS to FFT-APXPS in reconstructing signals readily done.

In Figure 31 I show (top) the time-resolved valence-band spectrum in the gas phase, along with (middle) the Fourier Transformation thereof and (bottom) the reconstructed spectrum obtained via inverse Fourier Transformation. The hatching shows the regions in the Fourier Transform whence I used signal to obtain the reconstruction shown in (bottom). Note that the phases may be slightly offset with respect to each other between the binding energy regions which were stitched together. I have attempted to correct for this by offsetting the spectra themselves in the time direction before stitching, but this technique is not yet perfected, as it is still not algorithmically implemented, and leads to slight time-offsets. From the figure, we see that the durations of Surface Phases 1 and 2 are preserved also in terms of electronic structure variation.

It is relevant to note that the raw data signal is very clear even before any reconstruction is applied via inverse Fourier transformation, in contrast to the XPS images we have been examining in previous sections. In particular, it is easy to distinguish when the work function shift is in effect, and therefore for how long the gas pulse's effects last.

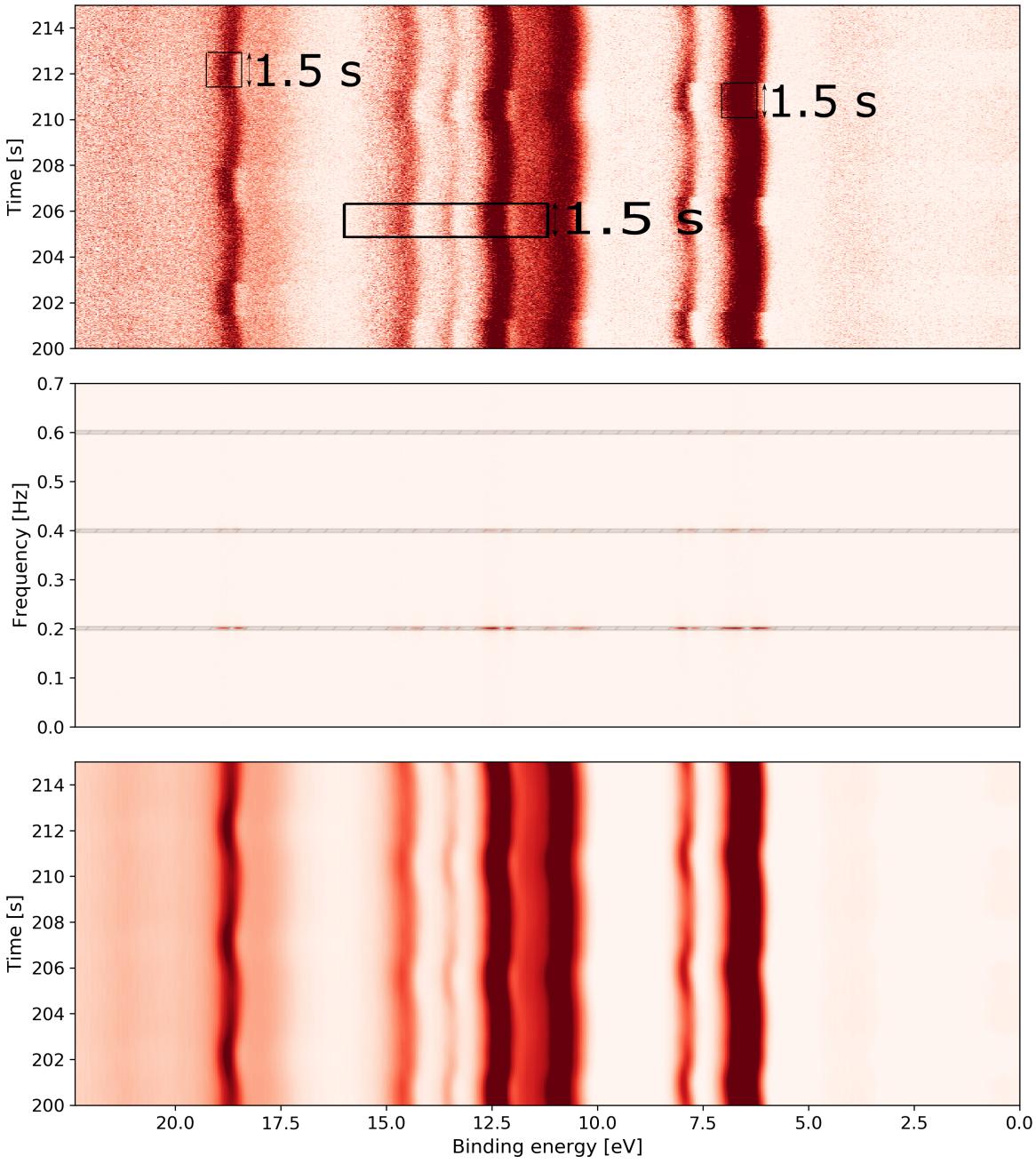

Figure 31: Figure showing (top) a 15 s snapshot of the time-resolved UPS spectrum in the valence band in the gas phase above the sample. (middle) shows the Fourier Transformation of the time-resolved UPS spectrum. (bottom) shows the reconstructed signal using inverse Fourier Transformation.

In Figure 32, I show the (blue) time-averaged UPS signal, with (gray shading) the oscillation in it, obtained from (green) the FT oscillation amplitude (multiplied by 3 for the purposes of the figure) at the fundamental frequency $f = 0.2$ Hz. The phase at this frequency is shown (dashed red) as well. On the basis of this figure and the comparison shown in Figure 30 I can assign the peaks in the gas phase. The feature in the average spectrum at 18.75 eV is due to oxygen in the gas phase. The feature at 14.6 eV is again due to oxygen, while the feature at 13.5 eV is due to CO_2. The feature at 12.35 eV is due to oxygen again, while the small shoulder at 11.7 eV is due most likely to CO. At 10.88 eV we again have an Oxygen feature. At 7.9 eV is a CO_2 feature and at 6.5 eV we finally have another Oxygen feature. The work function shifts deserve particularly-close attention and will be discussed further below. The above observations, together with the measurements of the workfunction shifts are summarized in Table 1; the table is best considered in light of the information presented in the discussion.

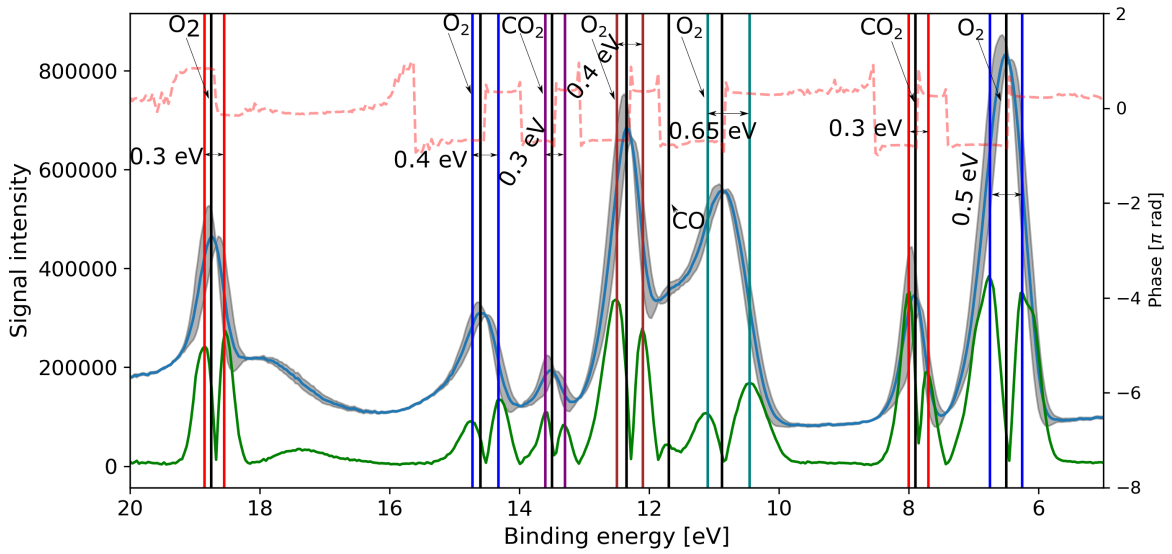

Figure 32: (Blue) The time-average UPS signal measured in the gas phase during CO oxidation on Pt(111). (Green) The FT oscillation amplitude is shown at the fundamental frequency $f = 0.2$ Hz, along with its (dashed red) phase. The FT spectrum is multiplied by 3 to provide a better visual reference. The gray shading shows the effect of the oscillation on the average signal. The features in the average spectrum, along with the workfunction shift in the FT spectrum are indicated.

Puglia et al. [32] have previously investigated the valence band UPS spectra of oxygen adsorbed on Pt(111) and we can therefore relate our findings to theirs. In particular, our spectrum matches theirs for the O_2 gas phase, with some small shift (Figure 5 of the cited work).

We now proceed to examine the surface valence-band spectra under reaction conditions. In Figure 34 I show as in the gas-phase case (top) the time-resolved spectrum, (middle) its Fourier Transformation and (bottom) the reconstructed spectrum obtained via inverse Fourier Transformation.

Again with the help of Figure 30, I assign the peaks in the time-average signal, which is shown (blue) in Figure 33, together with the oscillation in it (gray shading), the FT oscillation amplitude (green) at the fundamental frequency, from which the oscillation was obtained, and (dashed red) the phase of the FT.

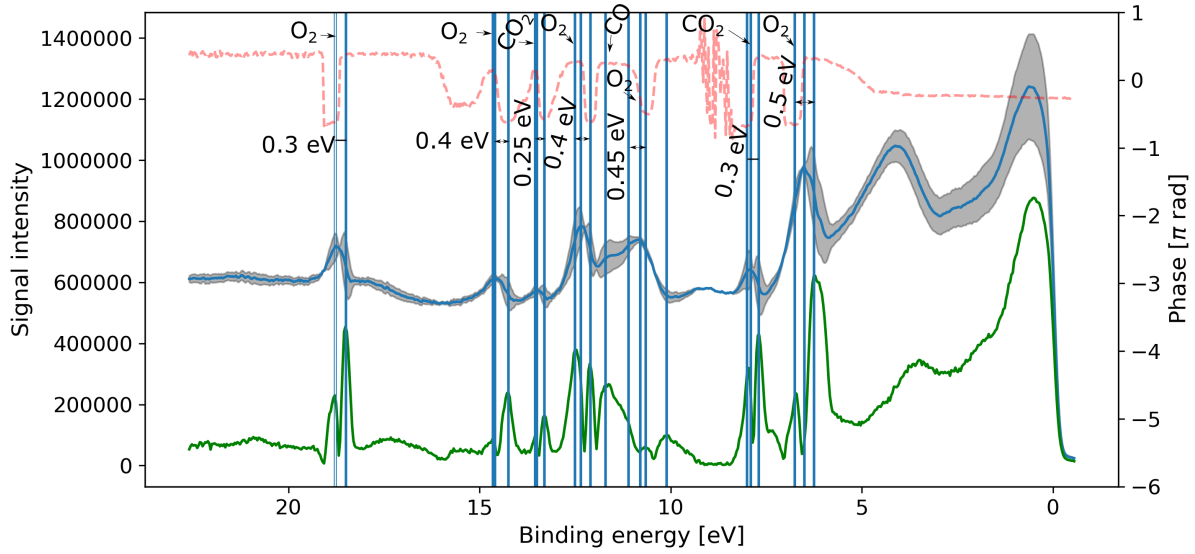

Figure 33: (Blue) The time-average UPS signal measured at the sample surface during CO oxidation on Pt(111). (Green) The FT oscillation amplitude is shown at the fundamental frequency $f = 0.2$ Hz, along with its (dashed red) phase. The Oscillation magnitude is multiplied by 8 to provide a better visual reference. The gray shading shows the effect of the oscillation on the average signal. The features in the average spectrum, along with the workfunction shift in the FT spectrum are indicated.

We see a peak due to oxygen in the gas phase above the surface at 18.75 eV. At 14.6 we see another oxygen component from the gas phase. At 13.55 is a CO_2 feature. At 12.35 is an oxygen feature. At 11.7 is the CO shoulder discussed above, but much more visible in this surface spectrum. This suggests that this feature is indeed due to CO adsorbed onto the surface. This hypothesis is supported by there being a feature at 11.8 eV in the nominally clean Pt spectrum of Figure 29. At 10.8 eV in the average spectrum we see a peak whose splitting is not immediately evident. The peaks in the shoulder at 11.1 eV and the one at 10.65 eV can be construed to come from the splitting of the 10.8 eV peak under the FT, which in turns means that that should be a gas-phase oxygen peak, which fits with the data from the gas phase.

At 10.1 eV, a peak is visible in the FT, though there is a trough in the average signal. This is particularly interesting, as it shows there is some oscillation in the local density of states even though no discernible peak which can be associated with a particular chemical species is visible.

At 7.9 eV and 6.5 eV in the average signal we again see peaks, and these are due to CO_2 and oxygen, respectively.

The observations above are summarized in Table 2.

Next, we proceed with a discussion of the UPS gas phase and surface spectra, with particular emphasis on the workfunction shifts exhibited by the peaks attributed to gas-phase species.

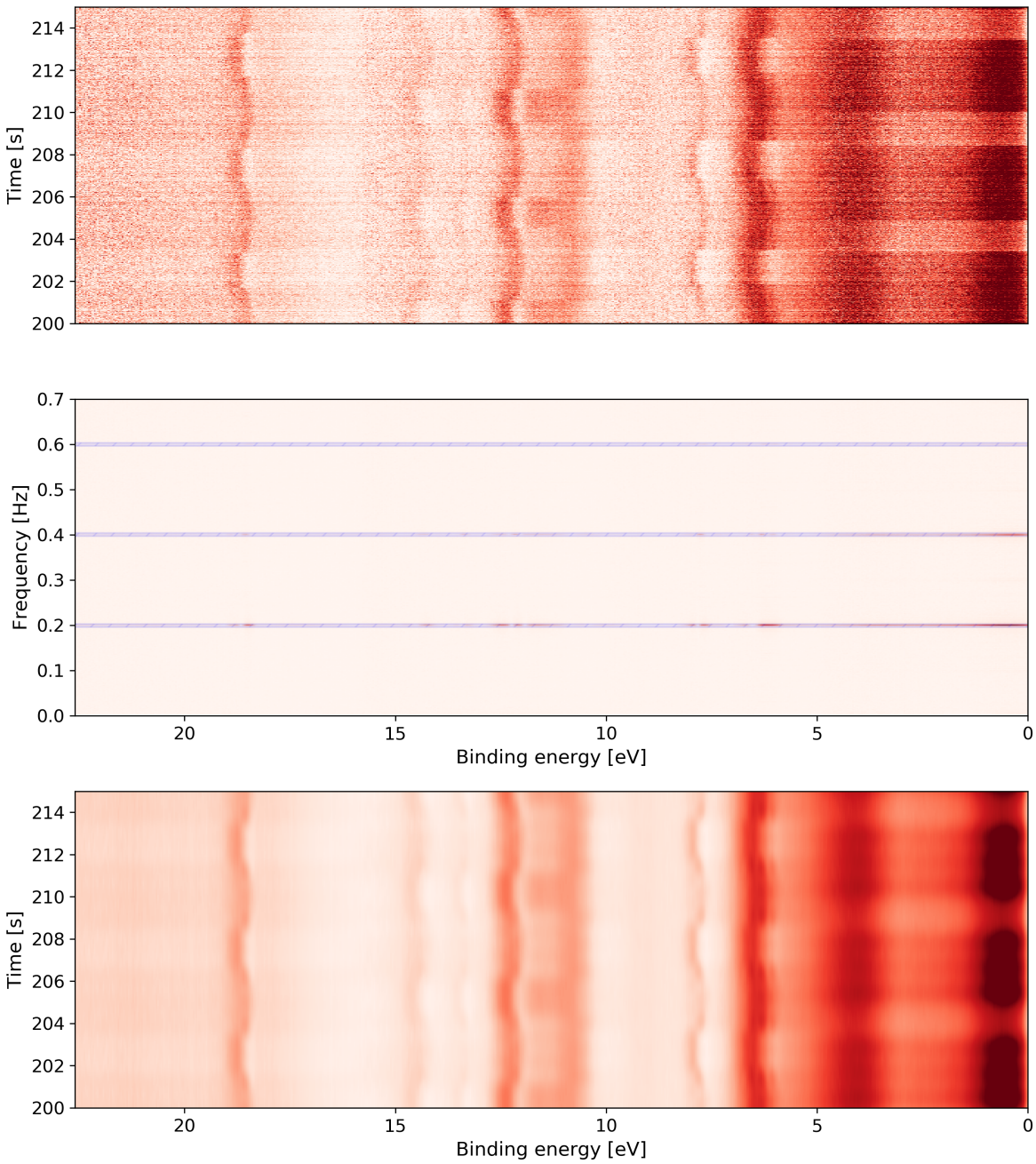

Figure 34: (top) shows a 15 s snapshot of the time-resolved UPS spectrum in the valence band in the surface position. (middle) shows the Fourier Transformation of the time-resolved UPS spectrum. (bottom) shows the reconstructed signal using inverse Fourier Transformation.

3.3.3 Discussion of valence-band spectra

The main thing to note is that the workfunction shift present in the FT peaks is *not* universally 0.4 eV. The locations of the peaks, along with the assigned chemical species, peak location in the average spectrum, peak locations in the FT image, and the resulting workfunction shift are summarized for the gas phase scan in Table 1. At 11.7 there is a shoulder feature, which I attribute to potentially

Table 1: Summary of the peak information from the UPS gas phase measurement during CO oxidation.

Species	Average spectrum peak [eV]	FT Peak 1 [eV]	FT Peak 2 [eV]	WF Shift [eV]
O_2 (g)	18.75	18.85	18.55	0.3
O_2 (g)	14.6	14.725	14.325	0.4
CO_2 (g)	13.5	13.6	13.3	0.3
O_2 (g)	12.35	12.5	12.1	0.4
CO (s?)	11.7	N/A	N/A	N/A
O_2 (g)	10.88	11.1	10.45	0.65
CO_2 (g)	7.9	8	7.7	0.3
O_2 (g)	6.5	6.75	6.25	0.5

Table 2: Summary of the peak information from the UPS surface measurement during CO oxidation.

Species	Average specturm peak [eV]	FT Peak 1 [eV]	FT Peak 2 [eV]	WF Shift [eV]
O_2 (g)	18.75	18.8	18.5	0.3
O_2 (g)	14.6	14.65	14.25	0.4
CO_2 (g)	13.5	13.55	13.3	0.25
O_2 (g)	12.35	12.5	12.1	0.4
CO (s)	11.7	N/A	N/A	N/A
O_2 (g)	10.8	11.1	10.65	0.45
CO_2 (g)	7.9	8	7.7	0.3
O_2 (g)	6.5	6.75	6.25	0.5

surface CO, as there is no split visible for it. (Since there is no split, it is either gaseous but only visible in one surface phase, or it is a surface species. The spectrum of Figure 29 suggests the latter)

The oxygen feature at 10.88 eV deconvolutes into FT peaks at 11.1 and 10.45 eV, for a large shift of 0.65 eV, while the feature at 6.5 eV, again due to oxygen, deconvolutes into FT features at 6.75 and 6.25 eV, respectively. This is a shift of 0.5 eV. While in the case of the feature at 10.88 eV this could potentially be due to interference in the image with the directly superimposed CO_2 feature, this is surely not the case for the feature at 6.5 eV, where a larger shift than 0.4 eV is observed.

I find no explanation for this behaviour at present, but contend that it is indeed a true, physical effect.

Finally, to facilitate comparison and to try and discern exactly what is happening on the surface in terms of electronic structure variation, consider Figure 35, where the difference in FT magnitude between the gas phase and surface position measurements is shown at the bottom. The top and middle panels show reproductions of Figures 32 and 33 without the spectral features marked. In the bottom panel, the FT peaks were manually adjusted to match between the gas and surface spectra where this was possible. The justification for this is that we are not trying to make a quantitative argument about signal ratios, but rather simply trying to discern which spectral features are specifically due to electronic state changes on the surface. Edge effects are visible due to the imperfect overlap of peaks, making it difficult to discern where the peaks in the difference spectrum are due to signal changes only in the surface position, and where they are due to errors in peak matching. I identify features at 11.52 eV and 7.4 eV (vertical lines) which seem to be due to real

effects. Therefore, we contend that this figure should be improved via more quantitative analyses.

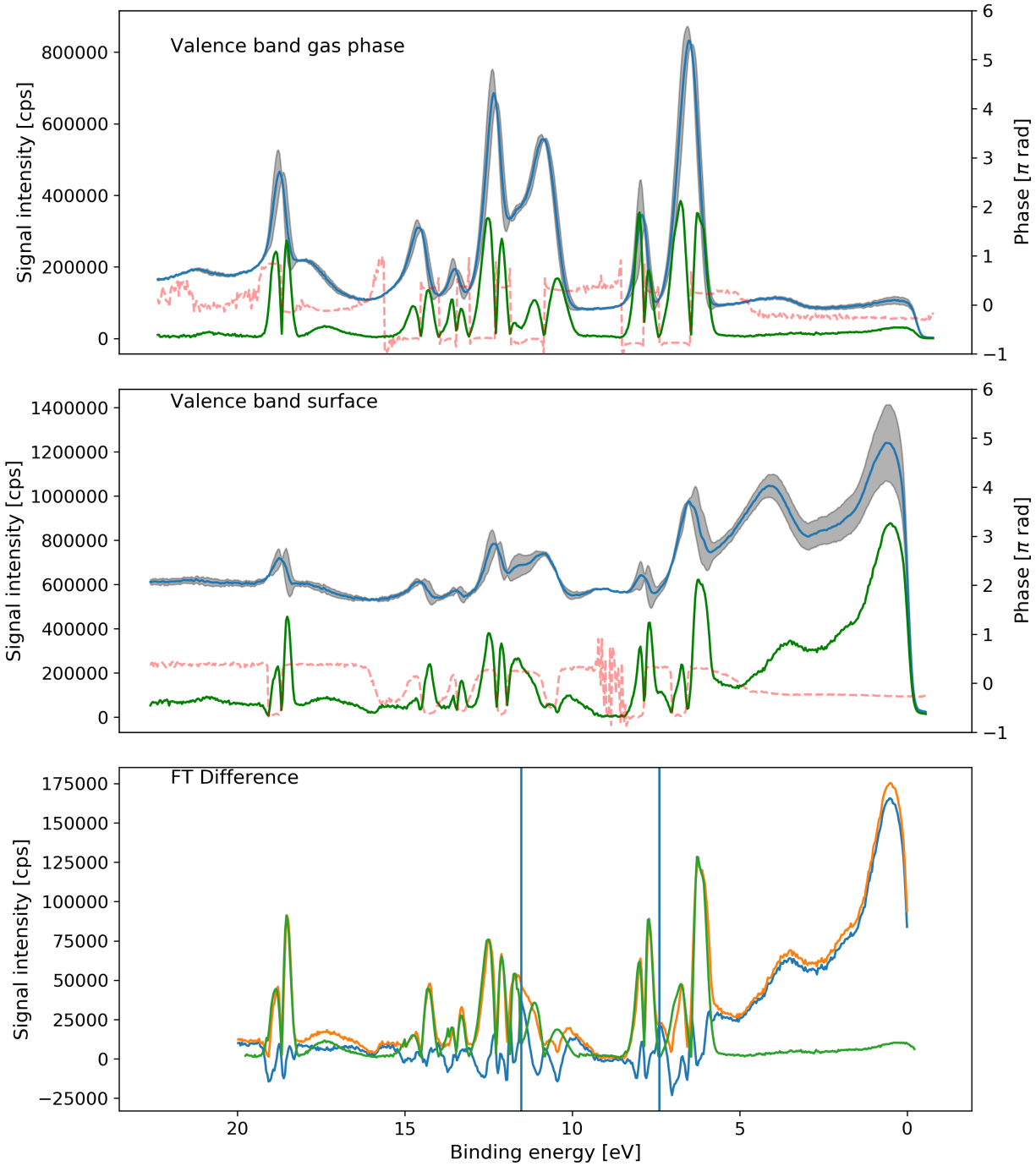

Figure 35: (top) shows the (blue) time-averaged UPS signal in the gas phase, with (green) the FT oscillation amplitude and (dashed red) the phase thereof. (middle) shows the same for the UPS signal in the surface position. (bottom) shows the difference (blue) between the UPS FT spectra in the gas phase and surface phase (orange and green), in an attempt to isolate surface oscillations.

On the basis of all the analyses performed above, I make several concluding remarks regarding the

information we can obtain from analyzing the valence band spectra. Firstly, the work function shift duration confirms the timings of 1.5 seconds in Surface Phase 2 and 3.5 seconds in Surface Phase 1 which we first noted when analyzing the core level spectra. Secondly, we again see evidence for CO adsorption onto the surface in Surface Phase 2, as we did when examining core level spectra. I do not find any feature which I can definitively attribute to oxygen adsorbed onto Pt. Therefore, we see that we can *corroborate most, but not all information* obtained from the core-level spectra. Crucially, were it only possible to examine the valence band data, we would not be able to discern whether the oxygen adsorbed onto the surface desorbs when the surface becomes CO poisoned.

We learned that there is an apparent difference in the workfunction shift between Oxygen and CO_2 in the gas phase, and overall we learned that the mathematical apparatus of FT-APXPS is suitable for investigations into the electronic structure of catalytic surfaces. We have, then, seen that the data visible in the valence band provides information in a compact way, enabling one to view contributions due to all chemical species in both the gas phase and on the surface in a compact binding energy range, enabling us to follow the dynamics of the surface phase oscillation in a comprehensive picture.

4 Discussion

First, we begin with some observations regarding aspects to be considered when interpreting FT-APXPS and FT-APUPS spectra. When looking at the FT magnitude, careful analysis of the phase of the signal is liable to yield additional insight. To wit, the width of spectral features visible in the FT Magnitude image can be estimated by considering how the phase behaves at the same binding energy. I have learned from practical experience that the phase signal is incoherent (i.e. oscillates wildly between all values) when there is no associated spectral feature at the same binding energy, that is, when only background secondary electrons are emitted or when there is no signal. This allows us to estimate the width and location of real features by the phase-space coherence length. Care must, however, be employed, as sometimes the phase of the background signal will, in fact, match that of a peak. Further refinement of the phase information may be a point of improvement in the technique.

Though the work on this experiment has been performed at a synchrotron facility, which enabled simultaneous evaluation of both the XPS and UPS spectra and therefore comparison thereof, the ideal course of development for the FT-APUPS technique is its use with lab-based sources. Therefore, the next step is to replicate the experiment with such sources and ascertain the following: 1) Is a sufficient photoelectron flux being generated with the typical laboratory-based source to perform UPS, and specifically FT-APUPS? 2) Can sufficient information be gathered in this case to make a quantitative, or at least qualitative judgment on how a catalytic reaction proceeds?

Another consideration is the fact that I have been performing the Fourier Transforms over the total number of time-resolved spectra. Instead, if one were interested in discerning whether, for instance, the integral of some particular peak changes during the course of the experiment, one could break up these spectra in subsets of spectra, say, the first 100 gas pulses, the middle section, and the final 100 gas pulses, or any variation thereof. That is, one can adjust the time-region where one performs the Fourier Transforms and limit it in such a way as to explore whether some irreversible change is occurring on the surface, whether transient effects are present during the first few pulses, etc.[4] Additionally, splitting up a total of N spectra into subsets of different sizes can confer more control over the trade-off in resolution between frequency and oscillation amplitude. To understand this,

[4]From discussions with my supervisor, I have learned that he has observed permanent non-periodic changes on a catalytic surface during the course of several surface phase transitions.

consider the following: if one were to take N spectra in time, one would obtain $N/2$ (or $N/2+1$) positive frequency bins under the Fourier Transform. If, however, one were to divide the N original spectra into, say, 4 subsets of $N/4$ spectra in time, one would then be able to perform a Fourier Transform on each subset, obtaining $N/8$ positive frequency bins. Clearly, this leads to a lower resolution in frequency space. However, one can then sum or average out the Fourier Transform magnitudes and thereby improve the signal to noise ratio.

As a final note on the usefulness of FT-APXPS/APUPS itself as a technique, we summarize the advantages when compared to traditional time-resolved methods: ability to precisely quantify the change in surface structure and thereby isolate the active surface phase from spectator phases, up to establishing precisely how much of the surface phase oscillates; the ability to reliably match the phases between which the surface oscillates in time; the ability to straightforwardly quantify work function shifts due to changes in surface phase; the ability to reconstruct the initial signal while filtering out irrelevant noise and frequencies; finally, the ability to precisely gauge the (energy-wise) size of spectral features via phase analysis.

Regarding the catalytic reaction itself, it is worth discussing whether we actually reach the mass-transfer limit. If the CO signal actually goes to zero, meaning that practically all CO introduced is converted into CO_2, we say that we are in the mass transfer limit. However, this is not necessarily the case as follows from our observations. In the C 1s (g) spectra, the CO signal goes very close to zero, but does not necessarily become zero. Furthermore, the CO structures on the Pt(111) surface do not completely disappear. Finally, the peaks in the valence band I attribute to CO in the gas phase do exhibit the 0.4 eV work function shift we see in all gas phase components. This lends credence to the argument that CO actually exists above the surface at all times, albeit with dips to very low concentrations. This would imply that we are essentially just at the edge of the mass transfer limit, occasionally perhaps dipping into it, but never fully in the situation that *all* CO is oxidized into CO_2.

Hence, given all the information gained in this work, through study via FT-APXPS and FT-APUPS, I suggest the following reaction mechanism at our pressure and temperature conditions: most of the surface is static, with a small percentage (between 2-7%) of it covered by adstructures which oscillate back and forth between one another. When the CO pulse is introduced, production of CO_2 increases and the workfunction shift induces a higher binding energy for the gas-phase components. This corresponds with an increase in CO/Pt-bridge and CO/Pt-atop coverage, as well as an increase in bare Pt atoms. This we called Surface Phase 2. After approximately 1.5 s, the coverage of said structures decreases, and we see an increase in the coverage of O/Pt-hollow structures, with a corresponding decrease in CO_2 production and hence catalytic activity. This we called Surface Phase 1, and it is associated with lower binding energy in the FT gas-phase peaks.

Another interesting aspect to note is that we do not observe any evidence of an oxide layer forming on the Pt(111) surface at any time. Indeed, such findings were reported, at higher pressures, for example, by Shavorksiy et al.[8].

In terms of outlook, several challenges which are left to be overcome in future works on FT-APUPS are worth discussing. Firstly, I have not proceeded to fit any spectra. In principle, it is straightforward to fit either the FT magnitudes alone, or the FT magnitudes together with the phase information obtained from the FT. This would allow for more reliable quantitative analyses of peak intensity ratios, chemical and work function shifts.

As noted, I found it relatively difficult to match the phase information in the case of stitched spectra when working with APUPS. This is because we have manually shifted the spectra before stitching.

Instead, an image recognition algorithm in the spirit of that used by Knudsen et al. in their work on event averaging can be employed in the following manner, assuming an overlapping binding energy region exists in the spectra: first, calibrate the spectra for transmission, as discussed in the methods section of this work; next, select this overlapping region or a subset thereof as a binding energy region of reference, and select a short time interval as a region of interest in time. Finally, shift one of the spectra in the time direction and subtract from it the other spectrum until the residual is smallest.

Another option to simplify the stitching process in terms of time-matching is to use an external trigger when recording the spectra, such that in each binding energy region the recording of the spectra commences exactly when an excitation arrives in the system. In the present case, this would entail triggering the detector when a gas pulse arrives, perhaps in a way similar to that achieved by Schavorskiy et al.

In the present work, the excitations inducing surface phase change were essentially pressure variations in the form of gas pulses. As an extension to this, it would also be interesting to look at temperature variations. Furthermore, the reaction pathway for CO oxidation is relatively simple, with only two reactants and one reaction products. Oxidation of more complex hydrocarbon molecules would be interesting to study, such as, for example, the oxidation of methane or ethylene. More reaction products and more complex reactants are liable to present a challenge in both the core energy level analysis as well as in the valence band analysis. However the payoff is likely to be an increased certainty in determining surface phase change owing to more distinct signatures of the various chemical species.

Finally, a speculative point. We have seen in Tables 1 and 2 that the work function shifts for the peaks observed in the valence band are not universally 0.4 eV, as was the case for the peaks observed in the core level spectra. In principle this could be due to observational or instrumental error, however the mismatch is systematic in the valence band and wholly absent in the core levels, and so I interpret this to be evidence for a differential work function shift depending on the nature of the molecular orbital which displays it. In particular, there are oxygen features with the expected shift of 0.4 eV, and features also due to oxygen which have shifts varying between 0.3 eV and 0.65 eV. Meanwhile, in the case of CO_2, we see three shifts of 0.3 eV and one shift of 0.25 eV, and in this case I find it weak evidence of differential shift. Hence, I believe the differential shift for O_2 is a real physical effect that should be investigated further.

5 Outlook and conclusion

In this work, I have demonstrated the usefulness of applying Fourier Transformations to data obtained in time-resolved Ambient Pressure X-ray photoelectron spectroscopy (FT-APXPS) and Ambient Pressure Ultraviolet Photoelectron Spectroscopy (FT-APUPS) experiments. I have examined the model catalyst system of CO oxidation on Pt(111) under in situ conditions in the context of a pulse-probe experiment, wherein CO gas was pulsed into a reaction cell with a constant background flow of Oxygen at pressures in the mbar regime and past the ignition temperature of the CO oxidation reaction.

By examination of the resulting FT-APXPS data, I have established the dynamics of surface phase oscillation at the edge of the CO mass transfer limit in this system. I have thereby validated previously-existing work on this model catalyst and found evidence that indicates the transition between a CO-poisoned and oxygen-poisoned surface, with a small population of clean metal patches.

Indirectly, this work therefore contributes to the ongoing debate on whether the catalytically-active phase of Pt(111) is oxide-covered, by showing that while a surface covered by chemisorbed oxygen is catalytically-active, there also exist patches of bare Pt present, therefore revealing the need for further investigation. I have thus validated the use of FT-APXPS on a new model catalyst. I have extended the use of FT-APXPS into the valence band, achieving the first use of FT-APUPS for investigations in model catalysis. I have established the limits of the method as used and suggested further improvements. Finally, I have identified a possible differential work function shift in the valence band region for oxygen adsorbed onto the Pt surface.

As I discuss in the previous section, future developments in the techniques of FT-APXPS and FT-APUPS are most likely to be in the direction of improved quantitative analysis. Furthermore, the elucidation of the apparent differential work function seen in some valence-band spectral features is likely to be of some interest.

The impact of this work is likely to be further refinement of FT-APXPS and FT-APUPS and a more thorough understanding of the dynamics between catalyst surface structure, electronic structure, and catalytic activity. In the long run, increased understanding of model and real catalyst systems are likely to bring about the development of more efficient and cheaper catalysts, thereby helping in increasing industrial efficiency and fighting against climate change.

References

[1] Alen Juginović, Miro Vuković, Ivan Aranza, and Valentina Biloš. Health impacts of air pollution exposure from 1990 to 2019 in 43 european countries. *Scientific Reports*, 11:22516, 11 2021.

[2] Joachim Schnadt, Jan Knudsen, and Niclas Johansson. Present and new frontiers in materials research by ambient pressure x-ray photoelectron spectroscopy. *Journal of Physics: Condensed Matter*, 32(41):413003, jul 2020.

[3] Matthijs van Spronsen, Joost Frenken, and Irene Groot. Observing the oxidation of platinum. *Nature Communications*, 8, 12 2017.

[4] S. Krick Calderón, M. Grabau, L. Óvári, B. Kress, H.-P. Steinrück, and C. Papp. CO oxidation on Pt(111) at near ambient pressures. *The Journal of Chemical Physics*, 144(4):044706, 01 2016.

[5] D. J. Miller, H. Öberg, S. Kaya, H. Sanchez Casalongue, D. Friebel, T. Anniyev, H. Ogasawara, H. Bluhm, L. G. M. Pettersson, and A. Nilsson. Oxidation of pt(111) under near-ambient conditions. *Phys. Rev. Lett.*, 107:195502, Nov 2011.

[6] Kai F. Kalz, Ralph Kraehnert, Muslim Dvoyashkin, Roland Dittmeyer, Roger Gläser, Ulrike Krewer, Karsten Reuter, and Jan-Dierk Grunwaldt. Future challenges in heterogeneous catalysis: Understanding catalysts under dynamic reaction conditions. *ChemCatChem*, 9(1):17–29, 2017.

[7] Jan Knudsen, Tamires Gallo, Virgínia Boix, Marie Døvre Strømsheim, Giulio D'Acunto, Christopher Goodwin, Harald Wallander, Suyun Zhu, Markus Soldemo, Patrick Lömker, Filippo Cavalca, Mattia Scardamaglia, David Degerman, Anders Nilsson, Peter Amann, Andrey Shavorskiy, and Joachim Schnadt. Stroboscopic operando spectroscopy of the dynamics in heterogeneous catalysis by event-averaging. *Nature Communications*, 12(1), December 2021. Publisher Copyright: © 2021, The Author(s).

[8] Andrey Shavorskiy, Giulio D'Acunto, Virginia Boix de la Cruz, Mattia Scardamaglia, Suyun Zhu, Robert H. Temperton, Joachim Schnadt, and Jan Knudsen. Gas pulse–x-ray probe ambient pressure photoelectron

spectroscopy with submillisecond time resolution. *ACS Applied Materials & Interfaces*, 13(40):47629–47641, 2021. PMID: 34590812.

[9] Dieter Baurecht and Urs Peter Fringeli. Quantitative modulated excitation Fourier transform infrared spectroscopy. *Review of Scientific Instruments*, 72(10):3782–3792, 10 2001.

[10] M. Roger, L. Artiglia, A. Boucly, F. Buttignol, M. Agote-Arán, J. A. van Bokhoven, O. Kröcher, and D. Ferri. Improving time-resolution and sensitivity of in situ x-ray photoelectron spectroscopy of a powder catalyst by modulated excitation. *Chem. Sci.*, 14:7482–7491, 2023.

[11] Taek-Seung Kim, Jeongjin Kim, Hee Chan Song, Daeho Kim, Beomgyun Jeong, Jouhahn Lee, Jae Won Shin, Ryong Ryoo, and Jeong Young Park. Catalytic synergy on ptni bimetal catalysts driven by interfacial intermediate structures. *ACS Catalysis*, 10(18):10459–10467, 2020.

[12] Philipp Müller and Ive Hermans. Applications of modulation excitation spectroscopy in heterogeneous catalysis. *Industrial & Engineering Chemistry Research*, 56(5):1123–1136, 2017.

[13] Veronica Bratan, Anca Vasile, Paul Chesler, and Cristian Hornoiu. Insights into the redox and structural properties of coox and mnox: Fundamental factors affecting the catalytic performance in the oxidation process of vocs. *Catalysts*, 12:1134, 09 2022.

[14] O. Björneholm, A. Nilsson, H. Tillborg, P. Bennich, A. Sandell, B. Hernnäs, C. Puglia, and N. Mårtensson. Overlayer structure from adsorbate and substrate core level binding energy shifts: Co, cch3 and o on pt(111). *Surface Science*, 315(1):L983–L989, 1994.

[15] N Johansson, M Andersen, Y Monya, J N Andersen, H Kondoh, J Schnadt, and J Knudsen. Ambient pressure phase transitions over ir(111): at the onset of co oxidation. *Journal of Physics: Condensed Matter*, 29(44):444002, oct 2017.

[16] B. N. J. Persson, M. Tüshaus, and A. M. Bradshaw. On the nature of dense CO adlayers. *The Journal of Chemical Physics*, 92(8):5034–5046, 04 1990.

[17] Sarah R. Longwitz, Joachim Schnadt, Ebbe Kruse Vestergaard, Ronnie T. Vang, , Ivan Stensgaard, Harald Brune, and Flemming Besenbacher. High-coverage structures of carbon monoxide adsorbed on pt(111) studied by high-pressure scanning tunneling microscopy. *The Journal of Physical Chemistry B*, 108(38):14497–14502, 2004.

[18] D. Frank Ogletree, Hendrik Bluhm, Eleonore D. Hebenstreit, and Miquel Salmeron. Photoelectron spectroscopy under ambient pressure and temperature conditions. *Nuclear Instruments and Methods in Physics Research Section A: Accelerators, Spectrometers, Detectors and Associated Equipment*, 601(1):151–160, 2009. Special issue in honour of Prof. Kai Siegbahn.

[19] Virginia Boix. *Graphene: Applications in Surface Science Studies.* Doctoral thesis (compilation), Synchrotron Radiation Research, October 2022. Defence details Date: 2022-12-02 Time: 13:15 Place: Rydbergsalen, Department of Physics. External reviewer(s) Name: Martín-Gago, José Ángel Title: Professor Affiliation: Instituto de Ciencia de Materiales de Madrid-CSIC (ICMM-CSIC) —.

[20] Nobelprize.org.Nobel Prize Outreach AB. The Nobel Prize in Physics 1924. `https://www.nobelprize.org/prizes/physics/1924/summary/`, 2023. Online; accessed 13 December 2023.

[21] Nobelprize.org.Nobel Prize Outreach AB. The Nobel Prize in Physics 1981. `https://www.nobelprize.org/prizes/physics/1981/summary/`, 2023. Online; accessed 13 December 2023.

[22] Chris Arble, Meng Jia, and John T. Newberg. Lab-based ambient pressure x-ray photoelectron spectroscopy from past to present. *Surface Science Reports*, 73(2):37–57, 2018.

[23] Samuli Urpelainen, Conny Såthe, Walan Grizolli, Marcus Agåker, Ashley R. Head, Margit Andersson, Shih-Wen Huang, Brian N. Jensen, Erik Wallén, Hamed Tarawneh, Rami Sankari, Ralf Nyholm, Mirjam Lindberg, Peter Sjöblom, Niclas Johansson, Benjamin N. Reinecke, M. Alif Arman, Lindsay R. Merte, Jan Knudsen, Joachim Schnadt, Jesper N. Andersen, and Franz Hennies. The species beamline at the max iv laboratory: a facility for soft x-ray rixs and apxps. *Journal of Synchrotron Radiation*, 24(1):344–353, 2017.

[24] Jan Knudsen, Jesper N. Andersen, and Joachim Schnadt. A versatile instrument for ambient pressure x-ray photoelectron spectroscopy: The lund cell approach. *Surface Science*, 646:160–169, 2016. Surface science for heterogeneous catalysis, a special issue in Honour of Richard Lambert.

[25] Joachim Schnadt, J. Knudsen, Jesper Andersen, H. Siegbahn, Annette Pietzsch, Franz Hennies, Niclas Johansson, Nils Martensson, Gunnar Ohrwall, Stephan Bahr, Sven Mähl, and Oliver Schaff. The new ambient-pressure x-ray photoelectron spectroscopy instrument at max-lab. *Journal of synchrotron radiation*, 19:701–4, 09 2012.

[26] Esko Kokkonen, Felipe Lopes da Silva, Mikko-Heikki Mikkelã, Niclas Johansson, Shih-Wen Huang, Jenn-Min Lee, Margit Andersson, Antonio Bartalesi, Benjamin N. Reinecke, Karsten Handrup, Hamed Tarawneh, Rami Sankari, Jan Knudsen, Joachim Schnadt, Conny Såthe, and Samuli Urpelainen. Upgrade of the SPECIES beamline at the MAX IV Laboratory. *Journal of Synchrotron Radiation*, 28(2):588–601, Mar 2021.

[27] Johansson, Niclas. The HPXPS Instrument at MAX-lab : a Powerful Tool for In Situ Catalysis Investigations, 2012. Student Paper.

[28] Küst, Ulrike. Linking the selectivity of varying surface phases of a real palladium catalyst toward specific methane oxidation pathways with Ambient Pressure X-ray Photoelectron Spectroscopy, 2023. Student Paper.

[29] S. Tanuma, C. J. Powell, and D. R. Penn. Calculations of electron inelastic mean free paths. ix. data for 41 elemental solids over the 50 ev to 30 kev range. *Surface and Interface Analysis*, 43(3):689–713, 2011.

[30] Tahereh G. Avval, Shiladitya Chatterjee, Stephan Bahr, Paul Dietrich, Michael Meyer, Andreas Thißen, and Matthew R. Linford. Carbon dioxide gas, CO2(g), by near-ambient pressure XPS. *Surface Science Spectra*, 26(1):014022, 07 2019.

[31] Christopher R. O'Connor, Jorge Anibal Boscoboinik, Mustafa Karatok, and Matthijs A. van Spronsen. Carbon monoxide, CO(g), by high-resolution near-ambient-pressure x-ray photoelectron spectroscopy. *Surface Science Spectra*, 27(1):014002, 02 2020.

[32] C. Puglia, A. Nilsson, B. Hernnäs, O. Karis, P. Bennich, and N. Mårtensson. Physisorbed, chemisorbed and dissociated o2 on pt(111) studied by different core level spectroscopy methods. *Surface Science*, 342(1):119–133, 1995.